



An-Najah National University
Faculty Of Engineering
Mechanical Engineering Department

Graduation Project II

Low speed wind tunnel- Design, Flow Simulation and
Manufacturing

Authors:

Mohammad Zayed, Mohammad Arafat, Sa'ad Tomeh, and Osaid Odeh

Supervisor: Eng. Luqman Herzallah

This project is presented as partial fulfillment of the bachelor's degree in
mechanical engineering

Submitted on 31 Dec, 2020

Abstract

Wind tunnel, a device that can provide a similar environment for objects moving through air, like a model of an aircraft. This process can provide a plenty of information on how a model can behave. Therefore, such an important testing device must be designed properly. A previous designed low speed closed wind tunnel must be checked to ensure that the right design was reached. The main purpose firstly to complete the entire design of the tunnel, this step was achieved by selecting an adequate measurement devices in order to determine a certain parameters. A strain gauge balance device was selected to measure the aerodynamic forces acting on a model like lift and drag forces, also pitching moment. The air flow over an object can be observed by many ways, smoke wire technique was followed, and by generating smoke the flow patterns could be seen. In addition, the hot wire technology was used to detect the air velocity anywhere inside the tunnel. Also, the design of major parts of the tunnel was tested by ANSYS Fluent separately, in order to determine the pressure and velocity of air at inlet and outlet for each part. The results of total pressure losses showed that there was an approximate correspondence between the theoretical and numerical approaches. Then, a scaled down wind tunnel was manufactured to conduct smoke visualization experiment.

Acknowledgements

The authors would like to thank Eng. Luqman Herzallah for his review and the support during preparing this report. Also a highly appreciated for Eng. Maher Na'eem Abu-Khadra and Eng. Fawzi Sadiq Abufarha for their technical report and following us for checking the wind tunnel design.

Contents

	Page
1 Introduction	9
1.1 The history of wind tunnel	9
1.2 Closed wind tunnel	11
1.3 Opened wind tunnel	12
1.4 Wind tunnel devices	12
1.4.1 Strain gauge balance	12
1.4.2 Hot wire anemometer	16
1.4.3 Smoke generation	16
1.5 Similarity	18
1.5.1 Geometric similarity	18
1.5.2 Kinematic similarity	18
1.5.3 Dynamic similarity	18
1.6 Aerodynamics experiments	19
1.6.1 Calibration	19
1.6.2 Flow visualization over various models	19
1.6.3 Pressure distribution over various models	19
1.6.4 Force measurement	19
2 Literature review	21
2.1 Background about the low speed wind tunnel design	21
2.2 Devices installation	22
2.3 Numerical approach	25
3 Methodology	26
3.1 Devices selection	26
3.2 ANSYS Fluent simulation	26
3.2.1 Geometry	26

3.2.2	Meshing	26
3.2.3	Setup	27
3.2.4	Solution	27
3.2.5	Results	28
3.3	Manufacturing stage	28
3.4	Limitations	29
4	Results and Discussions	30
5	Conclusion	35
	Appendix A	36
	Appendix B	41
	References	46

List of Figures

	Page
1.1 Benjamin Robins whirling arm (Baals 1981).	10
1.2 The first wind tunnel designed by Frank H.Wenham (Baals 1981).	10
1.3 Closed wind tunnel (NASA 2015).	11
1.4 Opened wind tunnel (NASA 2015).	12
1.5 Types of strain gauge balance according to placed location.	13
1.6 The definition of forces and moments for a body under uniform flow (White 2011).	13
1.7 A typical vane shape sketch showing the lift and drag forces with angle of attack (α) (White 2011).	14
1.8 Different mountings for aircraft model. (a) and (b) are for external balance, (c) and (d) are for internal balance (Hufnagel & Schewe 2007).	15
1.9 Hot wire anemometer probe (Jiang et al. 1994).	16
1.10 Flow visualization over square cylinder at different angles of attack (α), $Re_d = 6776$ (Sohankar et al. 2015).	17
2.1 A smoke wire location for an airfoil model in the test section (Batill & Mueller 1981).	22
2.2 An external triangle platform balance with six component (Samardžić et al. 2014).	23
2.3 Micro air vehicle has a 150 (mm) wingspan and equipped with a video camera (Samardžić et al. 2014).	24
2.4 The location of measurement points in the test section (Samardžić et al. 2014).	24
2.5 The locations of the apparatus for wind measurements (Maeda et al. 2011).	25
3.1 Final meshing for a separated wind tunnel parts.	27
4.1 Velocity profile for test section	31

4.2	Selected Hidria axial fan 350 (<i>mm</i>).	34
4.3	Final view of the scaled wind tunnel.	34
A.1	Dimensions for assembled closed wind tunnel (Abu-Khadra & Abofarha 2019).	36
A.2	Dimensions of separate parts for the wind tunnel (Abu-Khadra & Abofarha 2019).	37
A.3	Characteristic curve for Systemair axial fan selection (Systemair 2013).	39
A.4	Systemair axial fan ordering code (Systemair 2013).	40
A.5	Dimensions for Systemair axial fan (Systemair 2013).	40
B.1	Drag coefficient for three-dimensional objects (Gerhart et al. 2016).	42
B.2	TecQuipment's for wind tunnel balance for measuring lift and drag forces, and pitching moment (TecQuipment 2018).	42
B.3	Climomaster model 6501 hot wire anemometer product specification (KANOMAX 2019).	43
B.4	Hidria axial fan ordering code (Hidria 2020).	44
B.5	Dimensions for Hidria axial fan 350 (<i>mm</i>) (Hidria 2020).	44
B.6	Hidria axial fan 350 (<i>mm</i>) product specification (Hidria 2020).	45
B.7	Hidria axial fan 350 (<i>mm</i>) characteristic curve (Hidria 2020).	45

List of Tables

	Page
2.1 The applied roughness height and roughness constant for different parts of wind tunnel.	25
3.1 The dimensions for wind tunnel parts of original project with the scaled down by 4.	28
4.1 The Facent Average of velocity and total pressure at inlet and outlet for wind tunnels parts done by ANSYS Fluent.	30
4.2 The cost of original wind tunnel compared with the scaled one.	33
A.1 Theoretical results of pressure losses for wind tunnel parts (Abu-Khadra & Abofarha 2019).	38
A.2 Eckert experimental data for circular and square diffuser cross sections for calculating the local loss coefficient (Barlow et al. 1999).	38
A.3 Dimensions for several Systemair axial fan models in (<i>mm</i>) (Systemair 2013).	40
B.1 Typical balance materials (Hufnagel & Schewe 2007).	41
B.2 Specification for three-component balance (AF1300T) (TecQuipment 2018).	43

Nomenclature

F_D	Drag force (N)
F_L	Left force (N)
C_D	Drag coefficient
C_L	Left coefficient
ρ	Density (Kg/m^3)
U	Velocity (m/s)
A	Area (m^2)
Q	Flow rate (m^3/s)
α	Angle of attack
T	Temperature ($^{\circ}C$)
Re	Reynolds number
D	Characteristic linear dimension (m)
μ	Viscosity ($Pa.s$)
ν	Kinematic viscosity (m^2/s)
ΔP	Pressure loss (Pa)
P_{output}	Air power ($Watt$)
P_{input}	Fan input power ($Watt$)
η	Fan efficiency
K_f	Constant friction factor
K_e	Local loss coefficient
K_{exp}	Expansion loss coefficient
K_d	Diffuser loss coefficient
K_n	Nozzle loss coefficient
f	Friction factor
A_r	Area ratio
θ_e	Diffuser angle
K_S	Roughness height
C_{KS}	Roughness constant

Introduction

This chapter introduces the history of beginnings of the wind tunnel, the equipment and measurement devices that are located in the test section and the principle of their operation, wind tunnel similarity, and the experiments that can be conducted in the wind tunnel.

1.1 The history of wind tunnel

In the middle of eighteenth century (1700), airplane designers were trying hard to understand how objects can move properly in the air (Baals 1981). To achieve that purpose, they realized the essential understanding of air nature, and the way air could affect aircraft surfaces and how it moves around different types of shapes. At the beginning, they observed birds flight and tried to make aircraft similar shapes, unfortunately, birds did not give them the required data that enable to reach the desired design. They recognized that in order to get the required data they were ahead of two choices: moving the test aircraft through the air at the required velocity, or blowing air directly onto the object itself. The whirling arm was the first attempt to achieve their aim.

Benjamin Robins (1707-1751), an English mathematician, was the first researcher to employ the whirling arm (Baals 1981). His machine as shown in Figure 1.1 was just an arm of 4 feet long Spun by a falling weight acting on a pulley and spindle arrangement, the arm tip reached velocities of only a few feet per second. He has tested variously shaped objects by mounting them at the tip of the arm and spun them at different directions. Robins figured out the role of the shape on the movement and the resistance force (drag). Because of the arm could not reach more than a few feet per second, his experiments were limited. For years after that, researchers kept developing this machine in order to provide realistic tests to gather more accurate data. The whirling arm gave the researchers a good initial understanding of aerodynamics. However, it has a plenty of limitations that prevented them to reach the circumstances of the real flights.

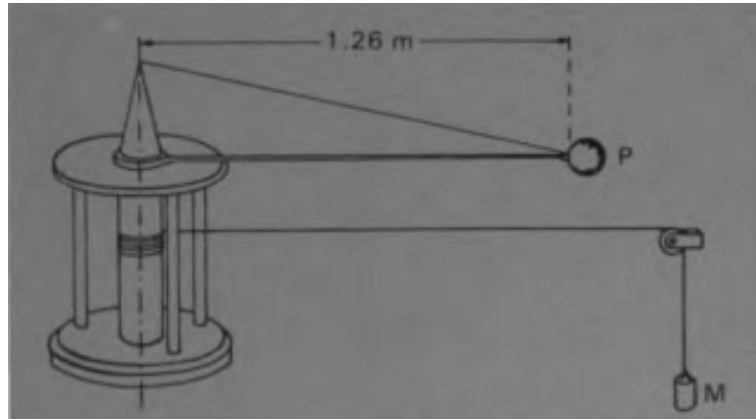


Figure 1.1: Benjamin Robins whirling arm (Baals 1981).

Researchers started to improve a dependable source of blowing air. The wind tunnel was the best solution. The wind tunnel solved the majority of whirling arm problems and a new era has begun (Baals 1981).

A wind tunnel simply is a device consist of an enclosed passage inside which the air is driven by a fan . The most important part is the test section, in which, a scale model is supported in a carefully controlled airstream (Baals 1981). Providing the possibility of gathering plenty of data about the model . The aerodynamic and flow characteristics are directly measured using a certain devices such as strain gauges and hot wire anemometer (Baals 1981). The wind tunnel has provided a way to measure the aerodynamic forces acting on a model. The three basic forces are lift, drag and side forces .

The first wind tunnel as shown in Figure 1.2 was designed by Frank H.Wenham in 1871 (Baals 1981). Because of failing in his experiment with the whirling arm, it was his motivation to make a new device. A different shapes and models were tested in this wind tunnel enabling Wenham to collect the lift and drag forces created by the air.

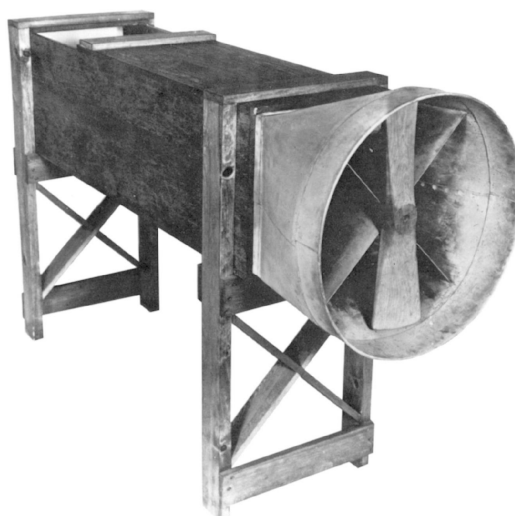


Figure 1.2: The first wind tunnel designed by Frank H.Wenham (Baals 1981).

Wind tunnels are built to achieve specific purpose. Therefore, there are several ways to classify wind tunnels. There are two basically types of them: closed and opened wind tunnel.

1.2 Closed wind tunnel

In this type of tunnels as shown in Figure 1.3, air passing after the test section returns to the fan by a series of turning vanes. The fan blow the air again into the contraction part and then air is back to the test section (NASA 2015). So, the air is continuously circulated inside the duct of closed tunnel.

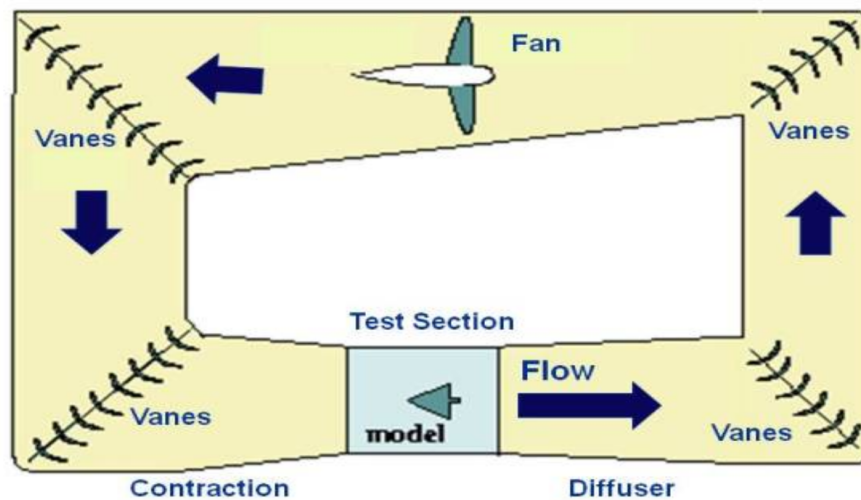


Figure 1.3: Closed wind tunnel (NASA 2015).

• Advantages of closed tunnel

1. Superior flow quality in the test section. The vanes at the corners and flow straighteners provide uniform flow through the test section (NASA 2015, Barlow et al. 1999).
2. Less energy required, thus low operating cost. Once the air is circulated, the fan just has to overcome the pressure losses through the walls and vanes (NASA 2015, Barlow et al. 1999).
3. More quiet than the opened tunnel (NASA 2015, Barlow et al. 1999).

• Disadvantages of closed tunnel

1. Costs more than the open because of added material (NASA 2015, Barlow et al. 1999).
2. In terms of propulsion and smoke visualization, it must be designed to purge exhaust products that accumulate in the tunnel (NASA 2015, Barlow et al. 1999).

1.3 Opened wind tunnel

This type has an open test section as shown in Figure 1.4. The air passing through the test section is gathered from the surrounding at where is the tunnel located (NASA 2015).

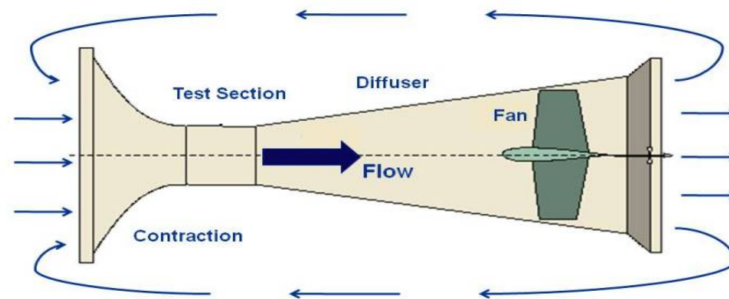


Figure 1.4: Opened wind tunnel (NASA 2015).

• Advantages of open tunnel

1. Low construction cost (NASA 2015, Barlow et al. 1999).
2. More efficient in propulsion and smoke visualization, there are no accumulation from the exhaust products (NASA 2015, Barlow et al. 1999).

• Disadvantages of opened tunnel

1. Poor quality flow in the test section (NASA 2015).
2. The fan must be continuously operating, leading to more energy to run, thus high operating cost (NASA 2015, Barlow et al. 1999).
3. Sounds noisy more than the closed (NASA 2015, Barlow et al. 1999).

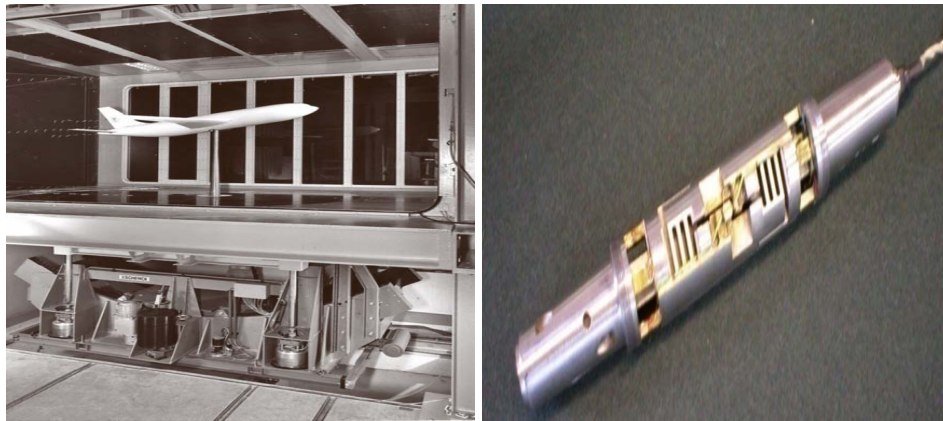
1.4 Wind tunnel devices

There are several instruments and measurement devices that are installed and located inside and outside the wind tunnel, specifically in the test section.

1.4.1 Strain gauge balance

A strain gauge balance (wind tunnel balance) is a device which used for measuring the aerodynamic forces. The principle work is based on the strain on an elastic material, and also it is a sensor whose resistance vary when applying loads. Strain gauges are called by that because they attached to elastic surface material (Ștefănescu 2020) . They can be found as

metal foils, semiconductors (thin film), piezoresistive (silicon), and also solid state devices. In case of wind tunnel measurements for aerodynamic forces, balance of wind tunnel can be classified according to the placed location, and the number of aerodynamic load components. In term of balance placed location, if the balance was located inside the model, it referred as internal balance. If it was located outside the model or either outside test section, it referred as external balance (Boutemedjet et al. 2018, Hufnagel & Schewe 2007). Figure 1.5a and Figure 1.5b shows the external and internal balance.



(a) External balance (Hufnagel & Schewe 2007). (b) Internal balance (Boutemedjet et al. 2018).

Figure 1.5: Types of strain gauge balance according to placed location.

In term of aerodynamic load components, it classified as one to six component strain gauge balance, three forces directed in coordinate axis and moment around these axis (Boutemedjet et al. 2018, Hufnagel & Schewe 2007). Figure 1.6 shows the forces and moments that can be measured are drag or axial force (acting on the main flow direction), lift or normal force (acting vertically to main flow direction) and side force. The moments are yaw, rolling and pitching moments (Boutemedjet et al. 2018).

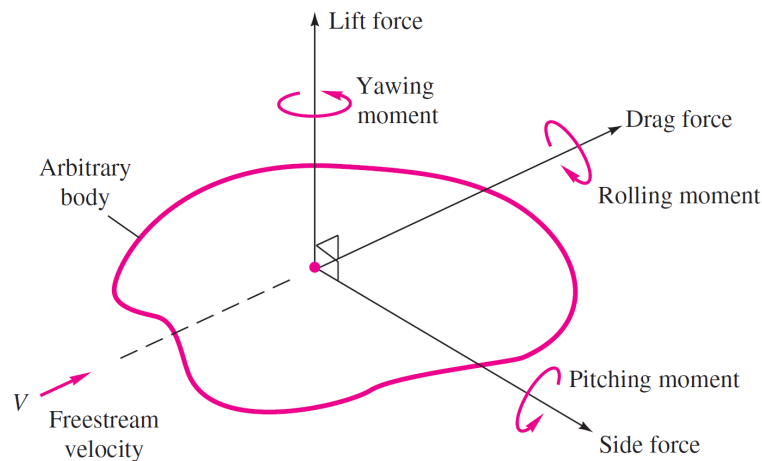


Figure 1.6: The definition of forces and moments for a body under uniform flow (White 2011).

The drag force depends on the drag coefficient, and that coefficient depends on the body shape (White 2011), Figure B.1 in Appendix B give some drag coefficients for different 3-D dimensional shapes. The lift force depends on the lift coefficient, and that coefficient depends on the angle of attack (α) (White 2011). Figure 1.7 shows the angle of attack for a vane shape with the direction of lift and drag forces. The drag and lift forces equations are shown in Equation 1.1 and Equation 1.2, respectively.

$$F_D = \frac{1}{2} C_D \rho U^2 A \quad (1.1)$$

$$F_L = \frac{1}{2} C_L \rho U^2 A \quad (1.2)$$

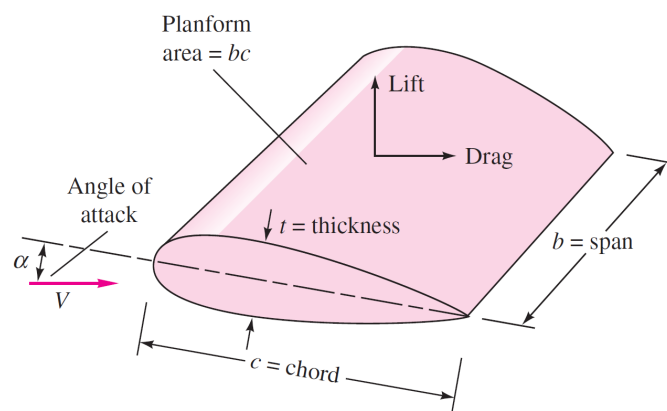


Figure 1.7: A typical vane shape sketch showing the lift and drag forces with angle of attack (α) (White 2011).

The strain gauge balance is the most one widely used in measuring force and moment in wind tunnel, the most used can be found as resistance foil strain gauge, or semiconductor gauge (Fan 2010, Hufnagel & Schewe 2007).

There are many supporting systems that were used for supporting the test model, it may have a mechanical system, which consist of a mechanism allow to adjust and control the altitude for model, an enough strength and stiffness should presented in the support system (Fan 2010). Strain gauge balance use a Wheatstone bridge that measure the electrical effect when the strain gauge deformed by applying balance load (Ștefănescu 2020, Fan 2010). High static pressure leads to relatively high load on the model.

There are many factors that must be take in the account when designing strain gauge balance, like the Mach number, type of wind tunnel, number of load components, accuracy of static calibration, the mass and center of mass for model, environmental factors (especially temperature), maximum allowable geometric dimensions of the balance and the connection between the balance and model (Fan 2010). The available space is not a limiting factor for external balance rather than internal balance which make it a major concern (Hufnagel & Schewe 2007).

Interference is one of the major systematic errors (which are errors repeated and occur every measurement, which eliminated by calibration) in wind tunnel balance caused by interaction of the model from the surrounding components, like when the axial component will collect some signal from the other loads components (Hufnagel & Schewe 2007).

There are various mounting support for models in wind tunnel for external and internal balances. A sting balance is the most used in the aerodynamic forces for low speed wind tunnel, the common forms are 'I' or 'T' beam shape (Fan 2010). In case of multi-component balance, it is important to arrange the balance correctly, in order to reduce the interference between each balance (Fan 2010). A sting can be mounted central and fixed inside the model as in Figure 1.8a (Hufnagel & Schewe 2007), or three sting support for an aircraft models as in Figure 1.8b, and more than three supports are required for buildings and cars (Fan 2010).

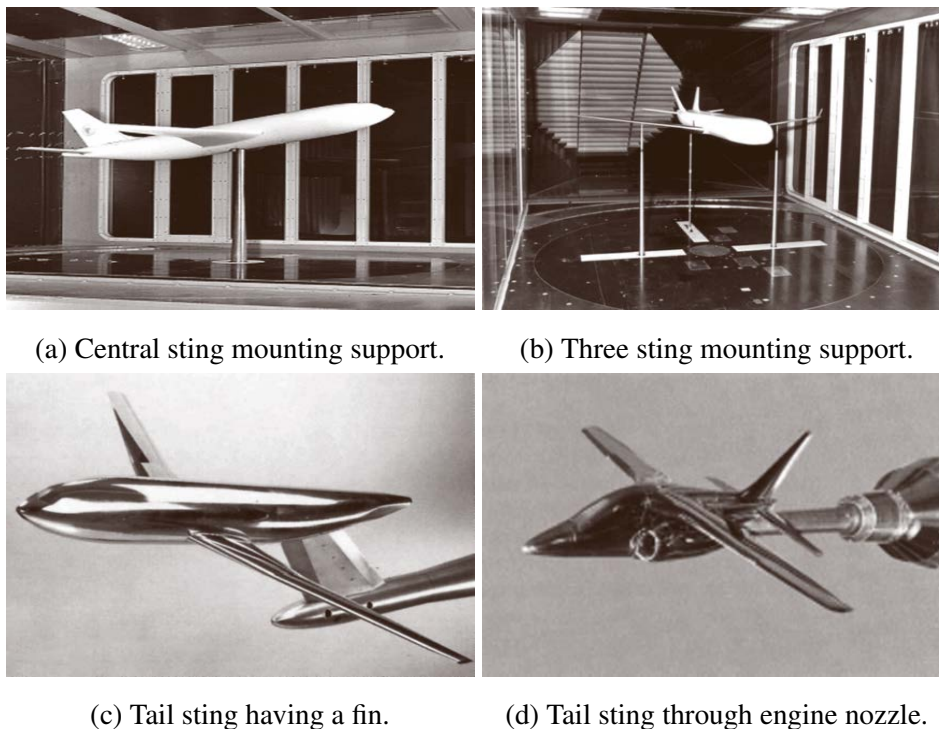


Figure 1.8: Different mountings for aircraft model. (a) and (b) are for external balance, (c) and (d) are for internal balance (Hufnagel & Schewe 2007).

It is important that all the loads must be carried by these supports and must be rigid to prevent the dynamic movement for the model during testing (Hufnagel & Schewe 2007).

The excitation voltage should be in a suitable range in order to get the desired output signal, but in the same time, it must not be higher than the range because higher excitation voltage will lead to heat up the strain gauge, which will leads to an errors (Hufnagel & Schewe 2007). A balance structure is made from metals, and the type of metal is depending on the stress level. Steel, titanium (used in aircraft) or copper-beryllium (having a high heat conductivity, which minimize temperature gradient) balance materials are used in high level stress, while aluminum used in low stress level. The yield stress for material selection must be three to five

times higher than the strain gauge stress itself (Hufnagel & Schewe 2007). The Table B.1 in Appendix B shows the mechanical properties for balance material.

A dynamic calibration used to check the performance and computational balance that performed in wind tunnel (Fan 2010). Static calibration is conducted on special calibration rig in order to obtain a relationship between the acting load and the output signal of the balance, which therefore to obtain a calibration formula (Fan 2010, Hufnagel & Schewe 2007).

1.4.2 Hot wire anemometer

Hot wire anemometer used for measuring the mean velocity components in turbulent flow in wind tunnels (Ristić et al. 2004, Barlow et al. 1999). A mechanism can be mounted outside the flow surface where the hot wire is placed (Barlow et al. 1999). It usually made from platinum (Jiang et al. 1994), it has a thin metallic sensors that heated up by electrical current when placed in flow field. The basic elements of hot wire anemometer is the probe where the sensors are appropriate placed on it and the electrical current in whetstone bridge for warming up the sensor (Ristić et al. 2004). The probe is fine wire as shown in Figure 1.9.

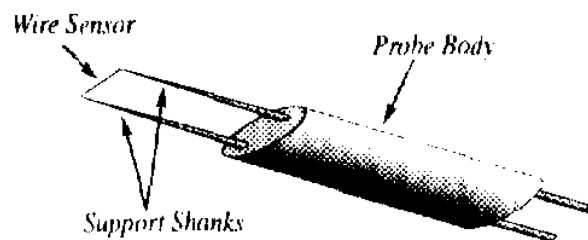


Figure 1.9: Hot wire anemometer probe (Jiang et al. 1994).

The sensor usually has the 0.038 - 0.005 (*mm*) diameter, with length from 1-2 (*mm*), and the sensor has a high temperature resistant coefficient and responds to changes in the total temperature (Ristić et al. 2004). In subsonic wind tunnel, where the temperature of fluid is low, which the heat transfer and the radiation effects will be ignored, the velocity is the only function the wire will respond (Barlow et al. 1999). So, a calibration process must performed by measuring the voltage across the bridge, in order to obtain the mean and turbulent velocities (Barlow et al. 1999).

1.4.3 Smoke generation

Flow visualization show the flow pattern around the surface of the model, and understand the nature also the phenomena of flow field (Lerner & Boldes 2011, Ristić 2007), and used to detect the unsteady flow characteristic (Sohankar et al. 2015), also used for experimental fluid mechanics in providing a picture of the flow field around scaled model and develop theories of fluid flow (Ristić 2007, Post & van Walsum 1993).

This visualization as shown in Figure 1.10 will detect the vortex flows, flow separation, and flow boundary layers (Ristić 2007, Garbeff & Bell 2019). Smoke is very useful in low speed wind tunnel.

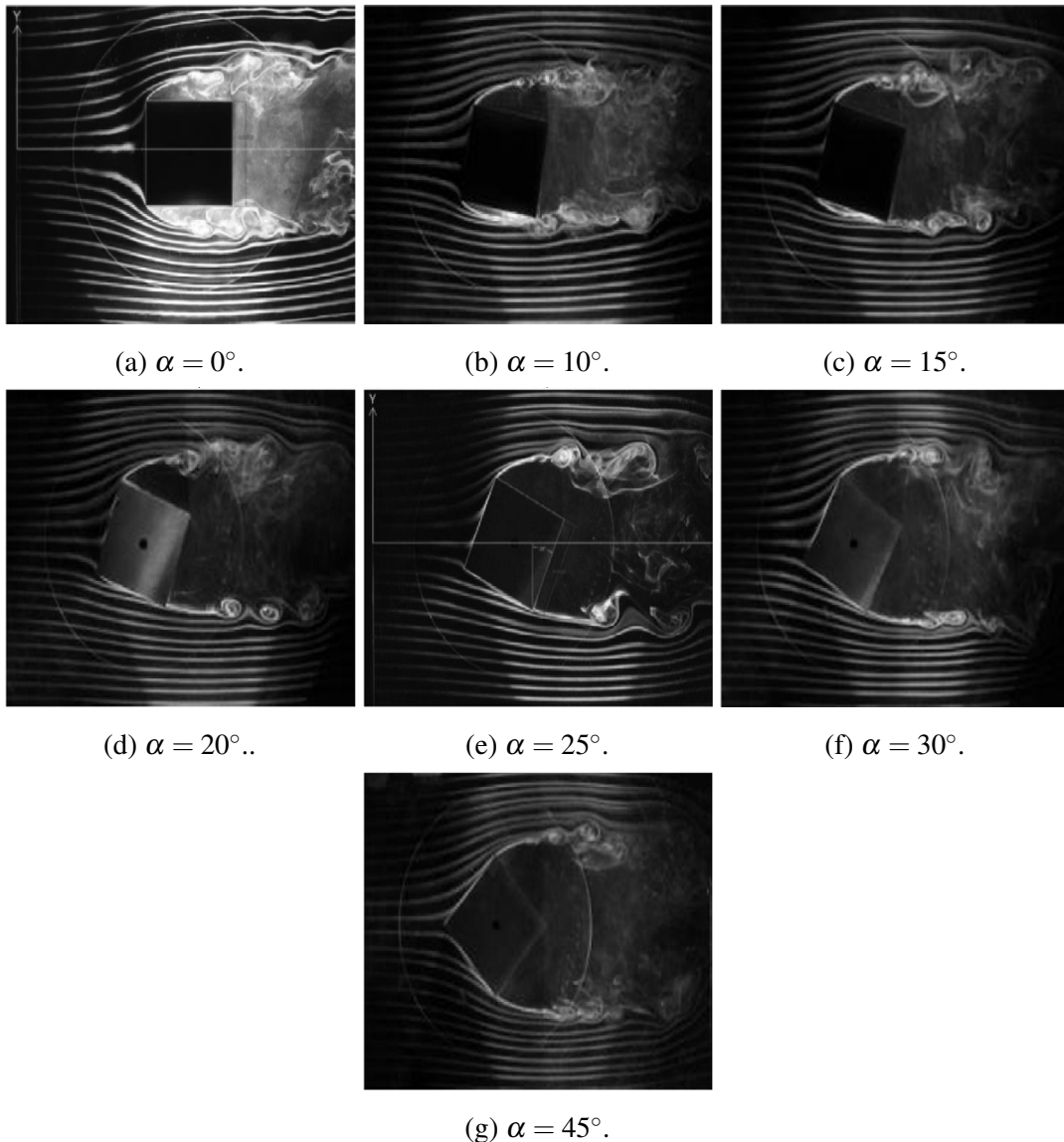


Figure 1.10: Flow visualization over square cylinder at different angles of attack (α), $Re_d = 6776$ (Sohankar et al. 2015).

There are many techniques for flow visualization, like smoke wire technique, laser light illumination technique and surface flow visualization technique (Lerner & Boldes 2011), but the most one will be talked about is smoke wire technique. The principle work of smoke wire technique is brushing a thin wire with oil manually, which therefore a small droplets will form, then the wire heated with the coated oil, which will evaporate the oil, and then with each droplet will make a fine streak line in the flow, this technique will require a fine wire (about 0.1 mm diameter) made from nickel chromium steel, and suitable oil in order to vaporized quickly, also a DC current to heat the wire (Lerner & Boldes 2011). The orientation of wire could be horizontally or vertically to main flow (Merzkirch 1987).

The smoke sources could be a vaporizing kerosene, propylene glycol oil (Lerner & Boldes 2011), or burning wood, tobacco or paper (Ristić 2007, Merzkirch 1987).

The smoke can be introduced through small pipes placed in the front of test model, there are several aspects when choosing the smoke in wind tunnel, like the smoke must be white and dense in order to be visible, also have to be a non-toxic and non-corrosive (Ristić 2007).

1.5 Similarity

For any specific reason, building a full-scale prototype become hard and even impossible. Therefore, instead of building a normal scale structure, a smaller one can be done. To make this smaller model, somethings must be taken to consideration in order to produce a good-scaled model from the prototype. Geometric, kinematic and dynamic similarities are required to be achieved allowing the model to have properties similar to the prototype.

1.5.1 Geometric similarity

It is achieved when two objects look exactly the same but they have different sizes. Geometrical similarity ensures that the ratios of prototype characteristics length to model lengths are equal. A model and prototype are geometrically similar if and only if all body dimensions in all three coordinates have the same linear scale ratio. In addition, all angles and flow direction are preserved (White 2011).

1.5.2 Kinematic similarity

It is a very important parameter that it must be achieved to complete the full similarity. It means that the velocity at any point in the model flow is proportional by a scale to the velocity at the same point in the full-scale one. Without geometrical similarity it cannot be done, the purpose of this similarity is to retain motion properties as the full-scale. A dimensionless parameter must be considered, keeping the same value of Reynolds Number is essential for the flow motion to save its properties (White 2011). Equation 1.2 shows the Reynolds number formula.

$$Re = \frac{\rho U D}{\mu} \quad (1.3)$$

1.5.3 Dynamic similarity

This type of similarity is a bigger term than the previous two, it means that to obtain the dynamic similitude, geometrical and kinematic similitude must be done firstly. If this approach was carried out properly, the model can produce a similar experiment circumstances as the bigger one. Because of these similarities, this ensures that all forces will be in the same ratio and have the same direction (White 2011).

1.6 Aerodynamics experiments

Many experiments can be performed in a wind tunnel. Each experiment has its specification and running condition depending on the desired output from it. These experiments are very important for the way of understanding objects movement through the air, in order to get the right desired design. Before doing any of these, a calibration experiment should be done.

The following experiments were taken from an Aerodynamic lab manual ([Dileep & Raghavendra 2018](#)).

1.6.1 Calibration

The main objective of the calibration is to measure the air velocity through the test section comparing with the fan speed. The apparatus of this test are an inclined tube manometer, multi tube manometer and pitot static probe. Thus velocity is calculated using inclined tube manometer at every RPM observed, also, velocity can be calculated using pitot static probe and multi tube manometer board.

1.6.2 Flow visualization over various models

The boundary layers are key parameters in aerodynamics, so, a flat plate can be used to determine the boundary layers thickness by using a boundary layers rake. By mounting the plate on a support at a specific position and connecting the static pressure ports of the plate to the multi-tube manometer. The boundary layer rake can be used to observe the boundary layers.

1.6.3 Pressure distribution over various models

In order to see how air flows over a body, a substance can be used to do this test. Smoke is a very good choice for the purpose of observing the air movement. A smoke generator used to deliver the smoke to the test section. A flow visualization test can be done to see the pressure distribution and separation points over a model.

A second test can be performed, a cylinder was tested to find the pressure distribution over it. The cylinder was mounted using wall mounting point and the pressure was measured using a pitot static tube. The same experiment can be done on a symmetrical air foil. The aim of such test is to know the flow nature around these bodies.

1.6.4 Force measurement

Another important experiment could be done on a certain object. A measurement of three component primary forces and moment over a general aircraft model can be performed using

6 component strain gauge on a model of an aircraft. By mounting the model in the test section at a specific position then setting the measurement device to cancel the weight effect, after turning on the fan, 3 component of force and 3 component of moment to be observed from the strain gauge.

In this report, the aim was to check the design of low speed closed wind tunnel in ([Abu-Khadra & Abofarha 2019](#)) using ANSYS Fluent software, and to select equipment and measurement devices, also to make-up a scaled down wind tunnel by similarity to be manufactured and conduct a smoke visualization experiment. A brief paragraph that described the parameters and principles of wind tunnel design will be found in chapter 2, also it included the related works and a review that describes the specifications of the equipment and measurement devices, the installation way in test section, the flow specifications like Reynold number and flow speed, also the parameters and assumptions that were used in ANSYS Fluent setup. chapter 3 talks about the research methodology, the way how to search on and select the measurement devices, also it included ANSYS Fluent worked sequence, manufacturing, and the limitations during this project. chapter 4 analyzed and compared the total pressure losses between the theoretical and numerical approaches, the sequence of similarity calculations and the measurement devices that have been selected. The last one will be talked about is chapter 5, which gave a summary of most important points and the results in this report, also a recommendations for future work.

2.1 Background about the low speed wind tunnel design

The preliminary design of low speed closed wind tunnel was designed by (Abu-Khadra & Abofarha 2019), Figure A.1 in Appendix A shows the dimensions of assembled closed wind tunnel, and Figure A.2 in Appendix A shows the separated wind tunnel parts. The test section was the starting point for designing close loop wind tunnel, which the other components were depending on it. As a start, for the test section, it was designed with $0.5 (m) \times 0.5 (m)$ square cross section area, having an air velocity with $30 (m/s)$, the length of the test section was 2 times the hydraulic diameter. For nozzle, the area ratio was selected to be 8 between the inlet and outlet, the cross section area for the outlet nozzle was equal to cross section area of test section. For second diffuser, the area of outlet diffuser was equal to nozzle inlet area, and the area of inlet diffuser was equal to fan inlet area, the area ratio between the fan and test section also the diffuser angle were 2 and 3, respectively. For first diffuser, the area of inlet diffuser was equal to test section cross section area, and the area of outlet diffuser was equal to fan inlet area. For the corners, which having square cross sectional area equal to first diffuser outlet area, it was having a 25 guiding vanes (bent flat plate type). The leading, trailing, and deflection angles were 5° , 0° , and 85° , respectively. For the honeycomb, the cell diameter, sheet metal thickness, length, and the roughness were $9 (mm)$, $0.06 (mm)$, $62 (mm)$ and $15 (\mu m)$, respectively. For the screens, the wire diameter and mesh divisions were selected to be $0.56 (mm)$ and $2.5 (mm)$, respectively. They have calculated the total pressure losses through all the components of wind tunnel which equal to $680 (Pa)$, and the flow rate at the test section was equal to $7.5 (m^3/s)$, and the suitable selected axial fan was AXC 630-9 2-pole type with a $12 (KW)$ power.

2.2 Devices installation

Smoke visualization is used to determine the behavior of flow around the model, there are some articles that describe the techniques used in order to have a proper smoke (including smoke-wire diameter), also the distance between the applied smoke and the model. (Gao & Liu 2018) had used a large capacitor as power source to heat the metal wire, oil droplets were attached to the wire, in order to heat the oil and vaporize it to make a smoke flow motion. A clear images shot for smoke streaks were taking at velocity $12.9 (m/s)$. (Batill & Mueller 1981) used a smoke wire technique at low Reynolds number ($50000 - 120000$) coated with oil, the test section length was $1.5 (m)$. The smoke wire location was at two positions from NACA 66-018 airfoil model, the horizontal position and was located $65 (mm)$ forward the leading edge of model, the vertical position was used to produce sheet of streak lines normal to leading edge and was located $430 (mm)$ forward of the leading edge of model as shown in Figure 2.1. A $0.076 (mm)$ smoke wire diameter made from 302 stainless steel was used with $0.4 (m)$ length and heated by power supply setting at $50 (V)$.

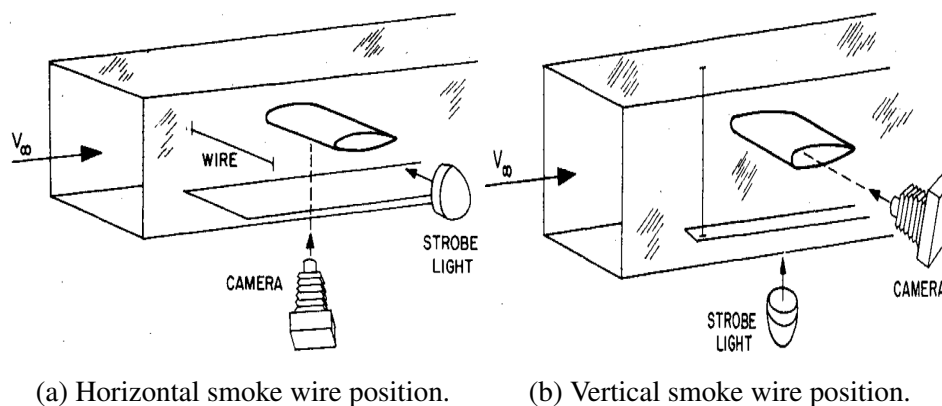


Figure 2.1: A smoke wire location for an airfoil model in the test section (Batill & Mueller 1981).

(Yarusevych et al. 2009) performed a flow visualization experiment in low turbulence wind tunnel for an airfoil model. The test section was $5 (m)$ long, $0.91 (m)$ wide and $1.22 (m)$ height, one of test section walls was made from Plexiglas for operational and visualization purpose. An aluminum airfoil (NACA 0025) with cord length $0.3 (m)$ was mounted horizontally at angle of attack $\alpha=5^\circ$. The smoke wires were installed vertically in the test section through $0.8 (mm)$ orifices in the wind tunnel walls, the position of wires was $5 (cm)$ offset from midspan plane. A $0.076 (mm)$ diameter wire made from 304 stainless steel was used, a glycerol based liquid was found the most effective smoke generation liquid, an optimum voltage was set to the coated wire to make smoke, the heat flux was $230 (KW/m^2)$ at $5 (m/s)$ air speed. The visualization was taken at $Re_c = 55 \times 10^3$, 100×10^3 and 150×10^3 .

A strain gauge used to determine the aerodynamics for the model, it is used to measure from one to six-components of forces and moments. According to (Belaidouni et al. 2018), the strain gauge balance is proportional to the aerodynamic component acting on the model, and

the electrical output is proportional to the applied forces and moments. The most common strain gauges are metal foil and semiconductor strain gauges. The foil strain gauge type is the most common used in wind tunnel experiments. (Samardžić et al. 2014) A six component external strain gauge (made from stainless steel) wind tunnel balance was designed in Military Technical Institute (VTI, Belgrade) to measure the drag, lift, and side forces, also yawing, pitching and rolling moments in test section with dimensions $0.4\text{-}0.6\text{ (m)} \times 0.4\text{-}0.6\text{ (m)}$, with velocity up to 50 (m/s) . A triangle platform balance was used as shown in Figure 2.2. A 6 (V) excitation voltage was used for the load cells, it was found that the loads for each component were not equivalent (do not have the same deflection). (Hanapur & Gopalakrishna 2016) Had

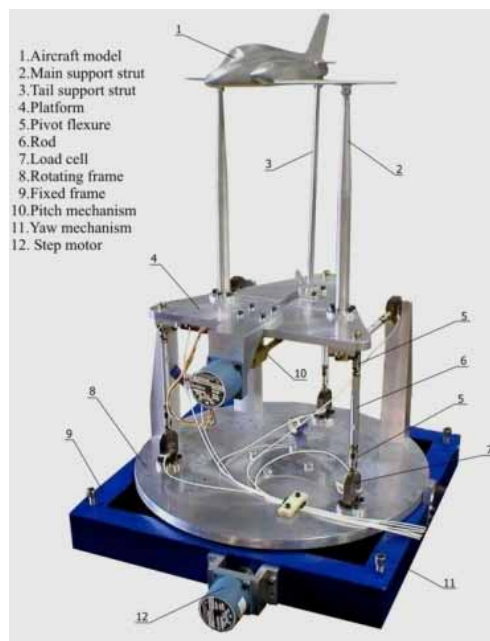


Figure 2.2: An external triangle platform balance with six component (Samardžić et al. 2014).

designed a 5-component internal strain gauge balance with a 25 (mm) diameter, a 17-4PH stainless steel material was used, it was designed for maximum stress $681\text{ (N/mm}^2\text{)}$, with minimum factor of safety 2. The model normally made from aluminum or stainless steel, loaded with a lot of sensors, a calibration process was used to record the output voltage when applying loads, in order to obtain voltage-load curve. By applying plot regression equation in Microsoft excel, the unknown loads will be determined when the output voltage of the load cell is known. (Orellano & Schober 2006) Had used an internal six component strain gauge balance to measure forces and moments on a leading car model made from aluminum and covered with foam plastic, the strain gauge was mounted on a special support device and was concentrated on the central attachment, the wind tunnel speed was varies from $30\text{-}70\text{ (m/s)}$, and Reynolds number was $0.6 - 1.4 \times 10^6$. (Albertani et al. 2007) Made a test on micro air vehicle (type of air craft) has a 150 mm wingspan as shown in Figure 2.3 on low speed and low turbulence wind tunnel at university of Florida, USA. The test section dimensions were $0.9\text{ (m)} \times 0.9\text{ (m)} \times 2\text{ (m)}$, the Reynolds number was having range between $(50000\text{-}150000)$.

A six component strain gauge with sting balance having a 10 (*mm*) diameter was used for aerodynamic forces and moments.



Figure 2.3: Micro air vehicle has a 150 (*mm*) wingspan and equipped with a video camera (Samardžić et al. 2014).

Hot wire anemometer used in wind tunnel to measure the airflow speed and located in the test section, it may require a mechanism which allow it to measure at different points. (Calautit & Hughes 2016) Had used a Testo 425 hot wire anemometer for measuring the vertical air flow velocity at inlet and outlet of an empty test section, and compare it with the CFD numerical software. The probe was controlled by a telescopic arm located through a hole drilled into the test section, in order to position the probe at the desired place as shown in Figure 2.4. A multiple measurements were taken until the temperature become stable in the wind tunnel to the ambient temperature $T=298$ (*K*), the velocities measurements were at speeds below 8 (*m/s*) and between 8-20 (*m/s*). (Maeda et al. 2011) Had used a T-type hot wire probe

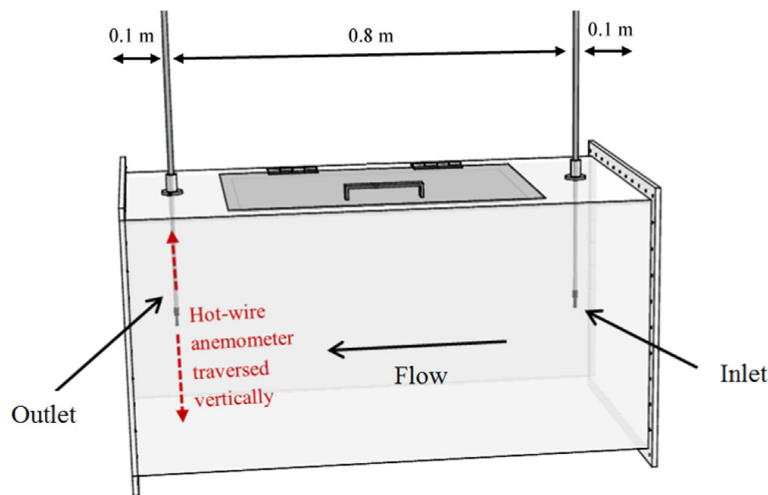


Figure 2.4: The location of measurement points in the test section (Samardžić et al. 2014).

for measuring the wind velocity and turbulence intensity for a horizontal axis wind turbine model, which has a two blades with $D= 500$ (*mm*) diameter. The open wind tunnel was having a 3600 (*mm*) nozzle diameter and $x= 6200$ (*mm*) test section length, the hub height was 2500 (*mm*) from the floor. The hot wire probe was attached on a positioning device as shown in Figure 2.5. The flow velocity was 7 (*m/s*), the velocity was measured vertically and horizontally at 6 positions at $x/D=1, 2, 3, 5, 7$ and 10 in range $-1000(\text{mm}) < y < 1000(\text{mm})$ with 40 (*mm*) interval. The measured velocity was an average at x-axial velocity. The y-axial

and z-axial velocities were not take in considered since they were much lower than the x-axial velocity.

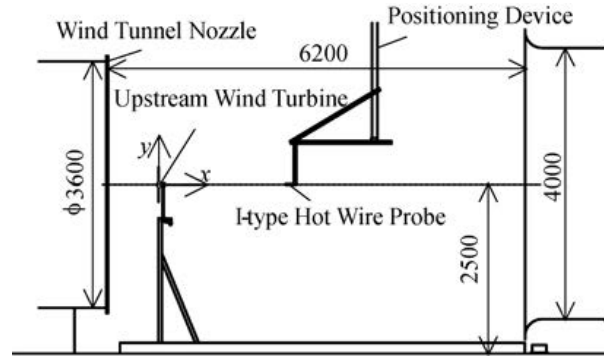


Figure 2.5: The locations of the apparatus for wind measurements (Maeda et al. 2011).

2.3 Numerical approach

A Computational Fluid Dynamics (CFD) software is a tool used to support wind tunnel design, wind tunnel testing, and test results. (Moonen et al. 2006) had used CFD as a numerical methodology to simulate the flow condition in low speed closed wind tunnel. A commercial ANSYS Fluent was used in (Calautit et al. 2014) to predict the flow characteristics in closed subsonic wind tunnel. For both (Calautit et al. 2014, Moonen et al. 2006), a standard K-epsilon turbulence model was used. The inlet pressure boundary was set for the inlet surface (intake fan) and was calculated as total pressure, the outlet pressure boundary was set to zero gauge pressure. The roughness height and roughness constant for all solid walls in the wind tunnel are shown in Table 2.1. For the solution method, a Semi-Implicit Method for Pressure-Linked Equations (SIMPLIC) velocity pressure coupling algorithm with second order was used, which solved by three-dimensional Reynolds Average Navier Stokes (RANS) equations in addition to continuity equation as presented in Appendix B. These equations can achieve approximate and realistic results by commercial software tools like CFD (White 2011).

Table 2.1: The applied roughness height and roughness constant for different parts of wind tunnel.

Related works	Boundary surface	K_S (m)	C_{KS}
(Moonen et al. 2006)	Floor, Wall, Ceiling and screen slats.	10^{-3}	0.5
	Guiding vanes.	10^{-6}	0.5
(Calautit et al. 2014)	Floor, Wall, Ceiling and guiding vans.	0.015×10^{-3}	0.5
	Test section surfaces.	0.0015×10^{-3}	0.5

This chapter describes the methodology to select wind tunnel devices, the way for using ANSYS Fluent to check the design of the previous project in ([Abu-Khadra & Abofarha 2019](#)), the manufacturing stage, and the limitations during this project, all of that organized as follow:

3.1 Devices selection

The selection of measurement devices and the way how they are mounted were looked out based on experiments in many researches and articles. The selection of the axial fan will based on the total pressure loss in the wind tunnel. The smoke generation will be selected based on smoke source, wire diameter and the distance between the smoke and the model. The selection of strain gauge balance will based on the type of support and drag force. The selection of hot wire anemometer will based of the range of air speed that will be measured.

3.2 ANSYS Fluent simulation

The ANSYS Fluent was learned by ([Fluent 2017](#)), and then was used to find out the total pressure loss in low speed wind tunnel, this was done under several stages as follow:

3.2.1 Geometry

First of all, the geometry was taken from previous project as SOLIDWORKS files as presented in Figure A.2 in Appendix A, then the Fill command was used to fill fluid inside geometry.

3.2.2 Meshing

Secondly, the fluid was meshed as shown in Figure 3.1 using Hexa/Prism method with fine element, then the boundary conditions were named as inlet, outlet, and walls.

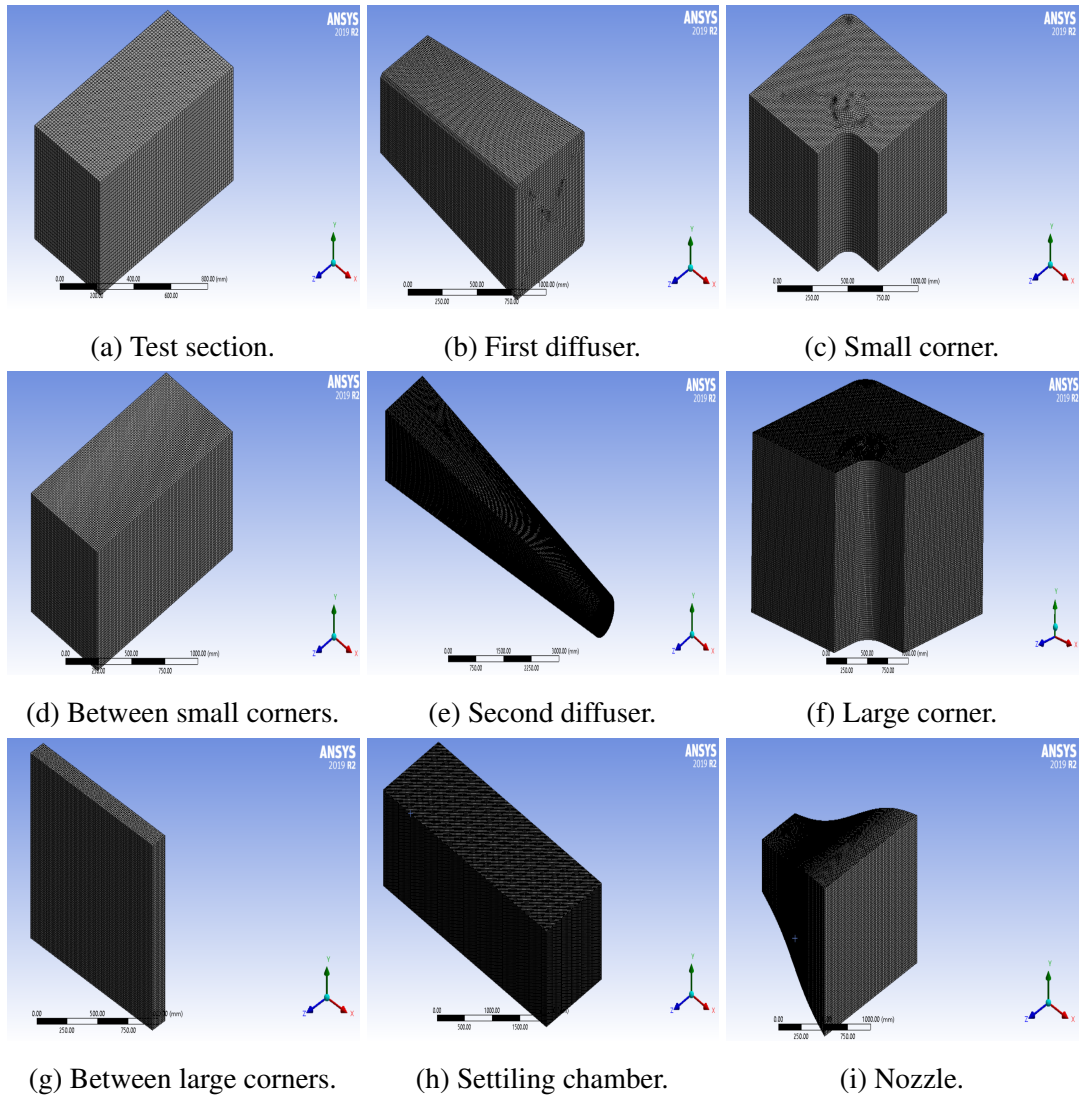


Figure 3.1: Final meshing for a separated wind tunnel parts.

3.2.3 Setup

The third process was Setup, which the viscous flow was defined as a standard K-epsilon (since the flow was turbulent). The density and viscosity (μ) for air at temperature $T = 20^\circ\text{C}$ were set $1.2047 \text{ (Kg/m}^3\text{)}$ and $1.8205 \times 10^{-5} \text{ (Pa.s)}$, respectively. The walls were defined as solid steel where the roughness height and roughness constant were $1.5 \mu\text{m}$ and 0.5 , respectively. The inlet boundary condition was set as inlet velocity, and the outlet boundary condition was set as outflow.

3.2.4 Solution

The fourth process was Solution, which defined the method for the solution. A SIMPLEC method with second order was selected. The solution was initialized from inlet, and the iteration was set at 1000 randomly.

3.2.5 Results

The Results were the final step, which used to find many parameters at certain boundaries. The velocity and total pressure at inlet and outlet were the most parameters that found as Facet Average. A velocity contour was used for test section to find out and examine the velocity profile.

3.3 Manufacturing stage

Because of certain reasons, a full-scale wind tunnel could not be built. Instead, a (1:4) scaled tunnel was designed and manufactured. This smaller one is simple and does not have options as the full-scale one. However, they share the same shape and geometry. The same concept and properties were followed. Even though the scaled model does not have features and ability to run tests as the normal one, the design process of smaller wind tunnel cannot be random, there were some important similitude procedures to be considered, geometrical, kinematic and dynamic similitude.

For geometrical similarity, all lengths for the full-scale tunnel were scaled to (1:4), making new small lengths to be manufactured as shown in Table 3.1. Some parts of the tunnel could not make it the exact value and were left to be later adjusted to ensure the tunnel will close. A proper fan were selected to fit the new distances and areas, and allows at least doing the smoking test.

Table 3.1: The dimensions for wind tunnel parts of original project with the scaled down by 4.

Wind tunnel parts	Original project		Scaled project		
		Cross section area (m^2)	Length (m)	Cross section area (m^2)	Length (m)
Test section		0.5×0.5	1	0.125×0.125	0.25
First diffuser	Inlet	0.5×0.5	1.48	Inlet	0.125×0.125
	Outlet	0.707×0.707		Outlet	0.175×0.175
Small corner		0.707×0.707	1	0.175×0.175	0.25
Between small corners		0.707×0.707	1.441	0.175×0.175	0.36
Second diffuser	Inlet	$\frac{\pi}{4} \times 0.797^2$	7.632	Inlet	$\frac{\pi}{4} \times 0.35^2$
	Outlet	1.414×1.414		Outlet	0.36×0.36
Large corner		1.414×1.414	2	0.36×0.36	0.5
Settling chamber		1.414×1.414	4.171	0.36×0.36	1.035
Nozzle	Inlet	1.414×1.414	1.41	Inlet	0.36×0.36
	Outlet	0.5×0.5		Outlet	0.125×0.125

The kinematic similarity is also important, and because of the geometrical similarity is completed, it can be done too. This can be happen if the Reynold number for the model flow remains as the prototype. After considering the same Reynold number, the velocity at the test section was calculated, relatively proportional to prototype test section velocity. The dynamic similitude is achieved simultaneously with the kinematic; also, the geometrical similarity allows the both to happen.

All parts of the model tunnel were made from 0.4 (*mm*) steel sheets, manufacturing them separately to be collected later. Also, a proper fan was selected and brought to fit at its place and to provide a good air circulation.

3.4 Limitations

There were some limitations while working with the ANSYS Fluent software. There were some wind tunnel parts that had not been tested, also the simulation for the whole wind tunnel has not been fully applied because this application needs a higher system requirements than the system that has been used. Also in term of mesh size and quality, the body mesh size that have been used was 15 (*mm*), and the mesh quality was excellent, but for a more accurate results, the mesh size must be finer and smaller than the size that has been used, this also needs a higher system requirements. On the other hand, strain gauge balance and hot wire anemometer were not available for doing some experiments. Instead, smoke visualization was the only experiment to be conducted.

Results and Discussions

Original project

Pressure losses

After the design was checked by ANSYS Fluent, the results in Table 4.1 show the inlet and outlet total pressure also the outlet velocity. Table A.1 in Appendix A shows the theoretical calculations results for the total pressure losses. The nozzle, first and second diffusers had wrong substitution during the calculation in (Abu-Khadra & Abofarha 2019), so these parts were recalculated as presented in Appendix A.

Table 4.1: The Facent Average of velocity and total pressure at inlet and outlet for wind tunnels parts done by ANSYS Fluent.

Wind tunnel parts	Inlet velocity (m/s)	Outlet velocity (m/s)	Total pressure at inlet (Pa)	Total pressure at outlet (Pa)	ΔP (Pa)
Test section	30	29.99	559.97	543.66	16.31
First diffuser	30	15.09	485.54	462.51	23.03
First corner	14.96	15.03	78.94	59.04	19.9
Between first and second corner	14.96	14.95	135.21	130.47	4.74
Second corner	14.96	15.03	78.94	59.04	19.9
Second diffuser	15	3.76	14.29	9.55	4.74
Third corner	3.75	3.78	4.81	3.59	1.22
Between third and fourth corner	3.75	3.74	8.52	8.51	0.01
Fourth corner	3.75	3.78	4.81	3.59	1.22
Settling chamber	3.75	3.74	8.51	8.00	0.51
Honeycomb	N/A	N/A	N/A	N/A	N/A
Coarse screen	N/A	N/A	N/A	N/A	N/A
Medium screen	N/A	N/A	N/A	N/A	N/A
Fine screen	N/A	N/A	N/A	N/A	N/A
Nozzle	3.75	30.03	522.05	512.25	9.8

Note: The results for Honeycomb, Coarse Screen, Medium Screen, Fine Screen and the simulation for whole wind tunnel are Not Available (N/A) because they need a higher system requirements.

There was an approximate agreement in the results between the numerical approach by ANSYS Fluent with the theoretical calculations, which justify the design of low speed closed wind tunnel.

Some parts have some difference in the results between the two approaches, this may be because of the approximation in the theoretical calculations, since the loss coefficient for some wind tunnel parts gave an approximate value for calculating the total loss due to friction, and changing the cross section area due to expansion and contraction. On the other hand, there was also an error in ANSYS Fluent results, since it gave a numerical and approximate results. Figure 4.1 shows the velocity profile for test section (not simulated with the whole wind tunnel), it can be notice that the velocity decreases when the flow approaches to the wall, and become zero at wall because of no-slip condition.

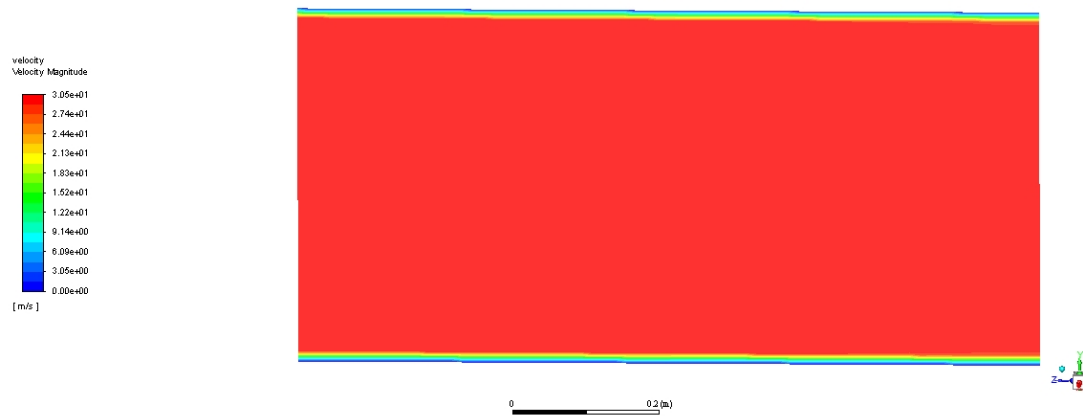


Figure 4.1: Velocity profile for test section .

Axial fan selection

The fan was selected from characteristic curve in Figure A.3 by the amount of the flow rate which was $7.5 \text{ (m}^3/\text{s)}$ and the total pressure losses which was about 121.7 (Pa) . The most suitable fan was AXC 800-9-4 (4KW) IE3 model, which will cover $7.7 \text{ (m}^3/\text{s)}$ and about 150 (Pa) total pressure loss. The description of the ordering code can be found in Figure A.4 in Appendix A. Table A.3 gave more details about dimensions for this fan corresponding with Figure A.5 in Appendix A.

Strain gauge balance selection

In order to determine a suitable strain gauge balance, at least, the drag force must be determined. A cubic model with 10 (cm) length was suggested for testing since it has a high drag coefficient as presented in Figure B.1 in Appendix B. The drag force was calculated as shown below:

$$F_D = \frac{1}{2} C_D \rho U^2 A$$

$$F_D = \frac{1}{2} (1.05) (1.2047) (30^2) (0.1 \times 0.1) = 5.7 (N)$$

A three-component balance (AF1300T) was selected as presented in Figure B.2 in Appendix B. Table B.2 in Appendix B has a more details about this balance.

Anemometer selection

A Climomaster model 6501 hot wire anemometer was selected, which can measure the air velocity between range 0.01-50 (m/s). Also, it can measure other parameters like pressure. Figure B.3 in Appendix B give more information about this device.

Scaled project

In order to make a scaled down wind tunnel (1:4), similitude was used. Geometric, kinematic and dynamic similarity are criteria must require to achieve the similitude.

Geometric similarity

All the dimensions were scaled down by constant scale number of 4, which was presented in Table 3.1.

Kinematic similarity

The streamlines for both model and prototype must be similar. So, the original wind tunnel will be called Model and denoted by (M). The scaled down wind tunnel will be called Prototype and denoted by (P). From dimensional analysis, we get Reynolds number. If the test section velocity for the model was 9 (m/s). By applying kinematic similarity, the velocity for the prototype will be determined as shown below:

$$(Re)_M = (Re)_P$$

$$\left(\frac{\rho U D}{\mu}\right)_M = \left(\frac{\rho U D}{\mu}\right)_P$$

The density and the viscosity are the same. So, the equation will be:

$$(U D)_M = (U D)_P$$

$$U_P = \frac{(U D)_M}{D_P} = \frac{9(0.5)}{0.125} = 36 (m/s)$$

So, the velocity at the prototype test section will be 36 (m/s), and the flow rate will be calculated as shown:

$$Q_P = (UA)_P = 36(0.125 \times 0.125) = 0.5625 (m^3/s) = 2025 (m^3/hr)$$

Dynamic similarity

In order to select a suitable axial fan, the pressure drop for the fan must be equal or greater than the static pressure. The axial fan product specification can be found in Figure B.6 in Appendix B. Calculations of the fan that will be used in the prototype should be based on the results of similitude. From axial fan characteristic curve in Figure B.7 in Appendix B, at 50 (Hz) and 2025 (m^3/hr) flow rate, the static pressure for the axial fan $\Delta P_{fan}=68.5 (Pa)$.

The overall efficiency of the axial fan is:

$$\eta = \frac{P_{output}}{P_{input}} = \frac{Q(\Delta P_{static})}{P_{input}}$$

$$29\% = \frac{0.5625 (\Delta P_{static})}{130} \rightarrow \Delta P_{static} = 67.02 (Pa)$$

$$\Delta P_{fan} = 68.5 (Pa) > \Delta P_{static} = 67.02(Pa)$$

Hidria axial fan R09-3530H-4M-4237 will be suitable for the scaled project. The description of the ordering code can be found in Figure B.4 in Appendix B. After the axial fan was selected as shown in Figure 4.3, the next step was the manufacturing. Table 4.2 shows the cost of the scaled wind tunnel. Figure 4.3 shows the final assembled scaled wind tunnel.

Table 4.2: The cost of original wind tunnel compared with the scaled one.

Wind tunnel components	Original project	Scaled project
	Manufacturing cost (NIS)	
Test section	320	20
First diffuser	540	50
Small corner	540×2	75×2
Between small corners	630	50
Second diffuser	4730	200
Large corner	2180×2	120×2
Settling chamber	3640	100
Nozzle	880	50
Axial fan	8800	260
Total price	16180	1120

Note: The cost of original project was based on 2 (mm) steel sheet, and the cost of scaled project was based 0.4 (mm) steel sheet.



(a) Front view.

(b) Back view.

Figure 4.2: Selected Hidria axial fan 350 (mm).



Figure 4.3: Final view of the scaled wind tunnel.

Conclusion

The simplest way is the best, for flow visualization, many methods were searched and the suitable was using the smoke from a certain smoke generator to allow the observation of the flow. The forces acting on a model are important, strain gauge balance was decided to be the appropriate way to measure all types of forces, with guaranteed and reasonable accuracy. For the purpose of measuring velocity and pressure at anywhere in the tunnel, the hot wire technology was the best way, providing multiple outputs from the same device. On the other hand, deciding these devices was slightly hard, regarding the availability in the local market or bringing them from outside.

For ANSYS Fluent simulation, parts that were simulated by the software turned up to be well designed and the mesh quality was excellent, and gave an approximately similar results as the theoretical approach, this means that these parts were good to be manufactured. On the contrary, there were some parts could not be tested. On the other hand, similarity was used to made up a scaled down wind tunnel, and an appropriate axial fan was selected to to achive the purpose of dynamic similarity. After that, the wind tunnel was manufactured and a smoke visualization experiment was conducted.

In future work, it would be better to simulate the entire wind tunnel by ANSYS Fluent software, this step ensures that the tunnel was well-designed. Unfortunately, such like huge operations need a super computers to be completed, which was not available. Also, it would be better to do more experiments like calibration and force measurement.

APPENDIX

A

This appendix will give briefly the previous design results in terms of wind tunnel dimensions, details about the axial fan that have been selected, and the total pressure losses with some modifications that were done by this report.

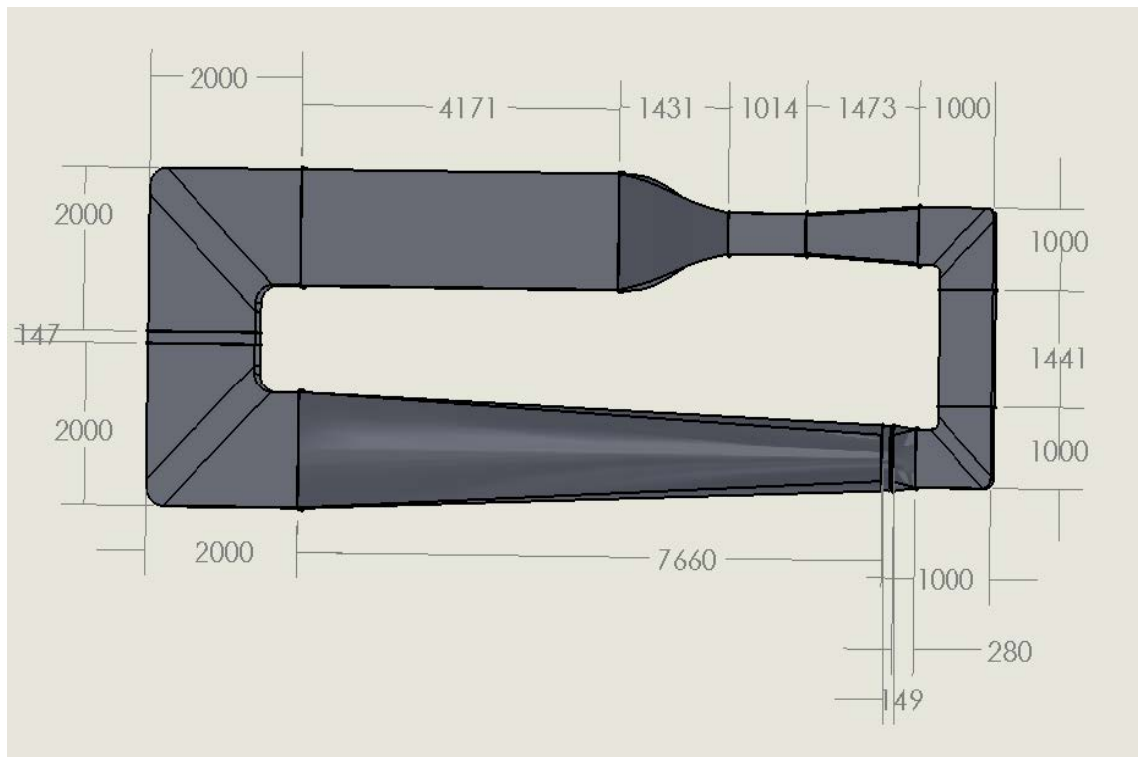


Figure A.1: Dimensions for assembled closed wind tunnel (Abu-Khadra & Abofarha 2019).

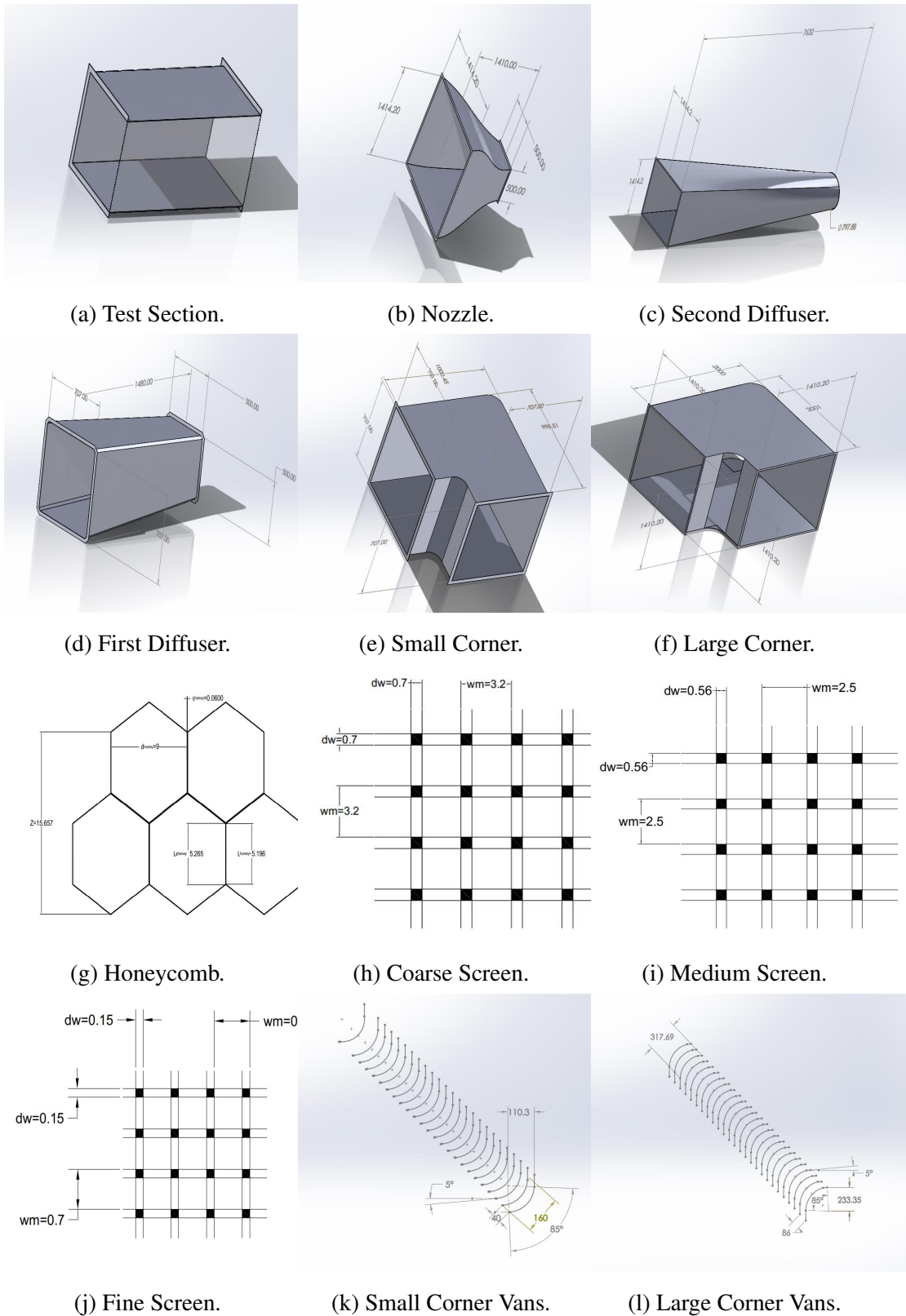


Figure A.2: Dimensions of separate parts for the wind tunnel (Abu-Khadra & Abofarha 2019).

Table A.1: Theoretical results of pressure losses for wind tunnel parts (Abu-Khadra & Abofarha 2019).

Components	ΔP (Pa)
Closed test section	11.8
First diffuser	461
Smaller corner	19.92
Constant-area section	0.0123
Smaller corner	19.92
Second diffuser	119.604
Larger corener	1.31
Constant-area section	4.95
Larger corener	1.31
Settling chamber	0.35
Honeycomb	16.946
Coarse screnn	7.715
Medium screen	8.08
Fine screen	5.3
Nozzle	2.05
Total pressure loss	680.6513

Note: First and second diffusers also nozzle had wrong substitution during solving the equations.

Table A.2: Eckert experimental data for circular and square diffuser cross sections for calculating the local loss coefficient (Barlow et al. 1999).

Parameter	Circular	Square
A_1	0.1033	0.09623
B_1	-0.02389	-0.004152
A_2	0.1709	0.1222
B_2	-0.177	-0.0459
C_2	0.0326	0.02203
D_2	0.001078	0.003269
E_2	-0.0009076	-0.0006145
F_2	-0.00001331	-0.000028
G_2	0.00001345	0.00002337
A_3	-0.09661	-0.01322
B_3	0.04672	0.05866

In Table A.1, first and second diffusers also nozzle were had wrong substitution while solving the equations in (Abu-Khadra & Abofarha 2019) design, so they were recalculated in this report as shown below:

First diffuser	Second diffuser	Nozzle
$K_f = \left(\frac{1}{A_e^2}\right)\left(\frac{f}{85\sin(\theta_e)}\right)$	$K_f = \left(\frac{1}{A_e^2}\right)\left(\frac{f}{85\sin(\theta_e)}\right)$	$K_n = 0.32f_{avg}\frac{L}{D_{sc}}$
$A_r = \frac{A_{outlet}}{A_{inlet}} = \frac{0.5}{0.25} = 2$	$A_r = \frac{A_{outlet}}{A_{inlet}} = \frac{2}{0.5} = 4$	$f_{avg} = 0.0119$
$\theta_e = 4^\circ$	$\theta_e = 3^\circ$	$K_n = 0.32(0.0119)\frac{1.41}{0.5} = 0.01074$
$f = 0.0119$ first factor for material	$f = 0.0123$ first factor for material	$\Delta P = 0.5K_n\rho U^2$
$K_f = \left(1 - \frac{1}{2^2}\right)\left(\frac{0.0119}{85\sin(4)}\right) = 0.0159$	$K_f = \left(1 - \frac{1}{4^2}\right)\left(\frac{0.0123}{85\sin(3)}\right) = 0.0275$	$\Delta P = 0.5(0.01074)(1.2047)(30^2) = 5.82Pa$
The equation for K_e (square)	The equation for K_e (square)	
$1.5^\circ \leq 4^\circ \leq 5^\circ$	$1.5^\circ \leq 3^\circ \leq 5^\circ$	
$K_e(\text{square}) = A_2 + B_2\theta_e + C_2\theta_e^2$ $+ D_2\theta_e^3 + E_2\theta_e^4 + F_2\theta_e^5 + G_2\theta_e^6$	$K_e(\text{square}) = A_2 + B_2\theta_e + C_2\theta_e^2$ $+ D_2\theta_e^3 + E_2\theta_e^4 + F_2\theta_e^5 + G_2\theta_e^6$	
From Table A.2	From Table A.2	
$K_e(\text{square}) = 0.41$	$K_e(\text{square}) = 0.2315$	
$K_{exp} = (K_e)(\theta_e)\left(\frac{A_r-1}{A_r}\right)^2$	$K_{exp} = (K_e)(\theta_e)\left(\frac{A_r-1}{A_r}\right)^2$	
$= (0.41)\left(4 \times \frac{\pi}{180}\right)\left(\frac{2-1}{2}\right)^2 = 0.0071$	$= (0.2315)\left(3 \times \frac{\pi}{180}\right)\left(\frac{4-1}{4}\right)^2 = 0.0153$	
$K_d = K_f + K_{exp} = 0.0159 + 0.0071 = 0.023$	$K_d = K_f + K_{exp} = 0.0275 + 0.0153 = 0.0428$	
$\Delta P = 0.5K_d\rho V^2$	$\Delta P = 0.5K_d\rho V^2$	
$\Delta P = 0.5(0.023)(1.2047)(30^2) = 12.47Pa$	$\Delta P = 0.5(0.0428)(1.2047)(15^2) = 5.8Pa$	

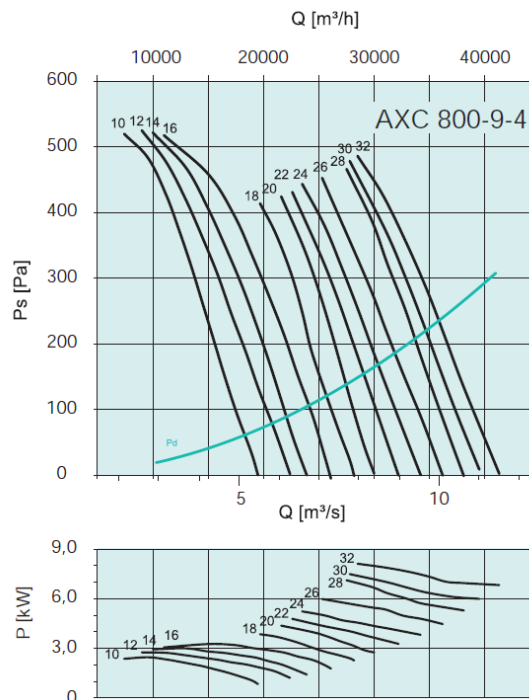


Figure A.3: Characteristic curve for Systemair axial fan selection (Systemair 2013).

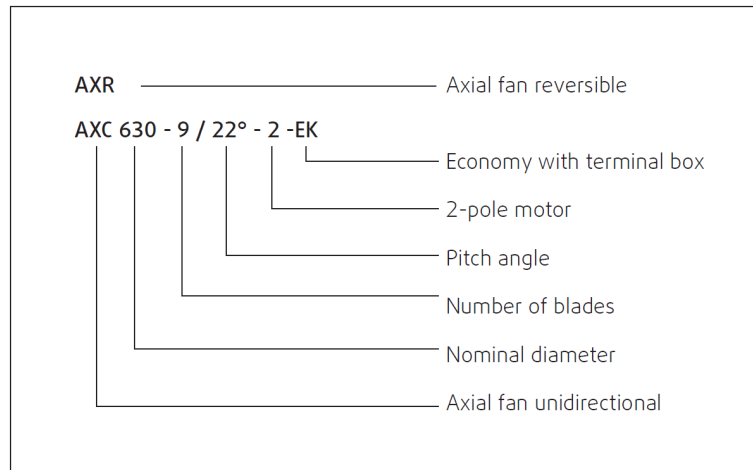


Figure A.4: Systemair axial fan ordering code (Systemair 2013).

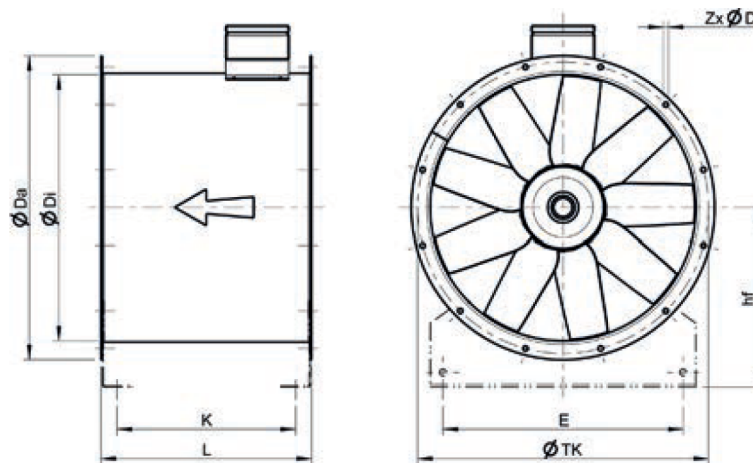


Figure A.5: Dimensions for Systemair axial fan (Systemair 2013).

Table A.3: Dimensions for several Systemair axial fan models in (mm) (Systemair 2013).

AXC	ϕDi	ϕDa	ϕTK	$Zx \phi D$	L	hf	E	K
AXC 315	315	395	355	8x 10	425	235	265	360
AXC 355	355	435	395	8x 10	425	250	305	360
AXC 400	400	480	450	8x 12	450	280	350	385
AXC 450	450	530	500	8x 12	500	315	400	435
AXC 500	500	590	560	12x 12	540	335	440	464
AXC 560	560	650	620	12x 12	500/750*	375	500	424/674*
AXC 630	630	720	690	12x 12	500/750*	425	570	424/674*
AXC 710	710	800	770	16x 12	500/700/800*	450	650	424/426/722*
AXC 800	800	890	860	16x 12	500/700*	530	730	414/614*
AXC 900	900	1005	970	16x 15	640/850*	560	830	552/762*
AXC 1000	1000	1105	1070	16x 15	640/850*	670	930	552/762*
AXC 1120	1120	1260	1190	20x 15	700/1000*	710	1030	612/910*
AXC 1250	1250	1390	1320	20x 15	850/1050*	800	1180	740/938*

* The dimensions of L + K depend on the motor frame size .

APPENDIX

B

This appendix will give more information and details about this report especially the devices specification that have been selected, which are strain gauge balance, hot wire anemometer, and an axial fan.

Table B.1: Typical balance materials ([Hufnagel & Schewe 2007](#)).

Material	Short name	Material number	Yield stress	Tensile stress	Young's modulus	Shear modulus	Density	Coefficient of heat expansion
			(N/mm^2)	(N/mm^2)	(N/mm^2)	(N/mm^2)	(Kg/m^3)	$(\mu m/mK)$
Maraging	X2 Ni Co Mo 18 8 5	1.6359	1760	1830	186000	71400	7920	11.6
Maraging	X2 Ni Co Mo 18 9 5	1.6354	1910	2010	191000	74600	8080	10.3
Maraging	X2 Ni Co MoTi 18 12 4	1.6356	2300	2400	190000	74600	8020	11.7
Maraging	X2 Ni Co Mo 18 8 3	1.6357	1430	1495	181300	68000	7920	9.0
Stainless	17-4-PH	1.4548	1170	1310	190000	75000	7780	10.0
Stainless	PH 13-8 Mo	1.4534	1150	1300	190000	75000	7760	10.0
Titanium	TI AL 6 V 4	3.7164	1000	1070	110000	43000	4430	8.6
Cu-Be	Cu Be 2	2.1247	1100	1500	123000	44000	8260	17.9
Aluminum	Al Cu Mg Mn	3.1354	300	430	72400	27600	2800	23.0
Aluminum	Al Zn Mg Cu Cr	3.4364	450	530	71000	27000	2800	23.0

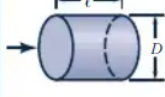
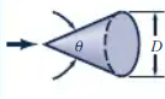
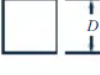
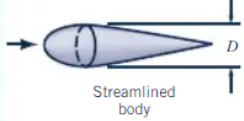
Shape	Reference area A	Drag coefficient C_D	Reynolds number $Re = \rho U D / \mu$										
 Solid hemisphere	$A = \frac{\pi}{4} D^2$	$\begin{matrix} \rightarrow & 1.17 \\ \leftarrow & 0.42 \end{matrix}$	$Re > 10^4$										
 Hollow hemisphere	$A = \frac{\pi}{4} D^2$	$\begin{matrix} \rightarrow & 1.42 \\ \leftarrow & 0.38 \end{matrix}$	$Re > 10^4$										
 Thin disk	$A = \frac{\pi}{4} D^2$	1.1	$Re > 10^3$										
 Circular rod parallel to flow	$A = \frac{\pi}{4} D^2$	<table border="1" data-bbox="890 611 997 707"> <thead> <tr> <th>U/D</th> <th>C_D</th> </tr> </thead> <tbody> <tr><td>0.5</td><td>1.1</td></tr> <tr><td>1.0</td><td>0.93</td></tr> <tr><td>2.0</td><td>0.83</td></tr> <tr><td>4.0</td><td>0.85</td></tr> </tbody> </table>	U/D	C_D	0.5	1.1	1.0	0.93	2.0	0.83	4.0	0.85	$Re > 10^5$
U/D	C_D												
0.5	1.1												
1.0	0.93												
2.0	0.83												
4.0	0.85												
 Cone	$A = \frac{\pi}{4} D^2$	<table border="1" data-bbox="890 745 997 842"> <thead> <tr> <th>θ, degrees</th> <th>C_D</th> </tr> </thead> <tbody> <tr><td>10</td><td>0.30</td></tr> <tr><td>30</td><td>0.55</td></tr> <tr><td>60</td><td>0.80</td></tr> <tr><td>90</td><td>1.15</td></tr> </tbody> </table>	θ , degrees	C_D	10	0.30	30	0.55	60	0.80	90	1.15	$Re > 10^4$
θ , degrees	C_D												
10	0.30												
30	0.55												
60	0.80												
90	1.15												
 Cube	$A = D^2$	1.05	$Re > 10^4$										
 Cube	$A = D^2$	0.80	$Re > 10^4$										
 Streamlined body	$A = \frac{\pi}{4} D^2$	0.04	$Re > 10^5$										

Figure B.1: Drag coefficient for three-dimensional objects (Gerhart et al. 2016).



(a) Three-component balance. (b) Digital display.

Figure B.2: TecQuipment's for wind tunnel balance for measuring lift and drag forces, and pitching moment (TecQuipment 2018).

Table B.2: Specification for three-component balance (AF1300T) (TecEquipment 2018).

Three-component balance (AFA4) with digital reading (AFA3)	
Electrical supply (Input)	100 VAC to 240 VAC , 50- 60 (Hz)
Operating environment	Laboratory
Balance dimensions	Width 480 (mm) × Depth 360 (mm) × Height 550 (mm)
Display dimensions	Width 140 (mm) × Depth 125 (mm) × Height 450 (mm)
Lift force	100 (N)
Drag force	50 (N)
Pitching moment	2.5 (N.m)
Air velocity	0-36 (m/s)

Note: This balance was designed and used for subsonic wind tunnel (AF1300) with 305 (mm) × 305 (mm) × 600 (mm) test section dimensions at Melton Keynes Collage, UK.

FEATURE		VALUE
Air Velocity	Range Accuracy Resolution	2 to 9840 FPM (0.01 to 50.0 m/s) *Varies by probe +/- 2% of reading or 0.015 m/s (whichever is greater) 0.01 m/s (0.01 to 9.99 m/s), 0.1 m/s (10.0 to 50.0 m/s)
Temperature	Range Accuracy Resolution	-4 to 158°F (-20 to 70°C) +/- 1.0°F (0.5°C) 1.0°F (0.1°C)
Humidity	Range Accuracy Resolution	2.0 to 98.0 %RH *Varies by probe +/- 2.0 %RH 0.1 %RH
Pressure (Optional)	Range Accuracy Resolution	-5.00 to +5.00 kPa +/- (3% of reading + 0.01) kPa 0.01 kPa
Interface	Digital Analog (Optional)	USB and RS232C (for print-out) DC 0 to 1 V (select one from Air Velocity, Temp, Humidity and Pressure)
Data Storage Capacity		Up to 20,000 records
Power Supply		6 x AA batteries or AC Adapter
Operation Range	Main Unit Probe Storage	41 to 104°F (5 to 40°C) with no visible condensation -4 to 158°F (-20 to 70°C) with no visible condensation 14 to 122°F (-10 to 50°C) with no visible condensation
Weight		0.9 lbs (400 g)
Dimensions		Main Body: 3.4 x 7.4 x 1.6 inches (88 x 188 x 41 mm)
Warranty		2 years



Figure B.3: Climomaster model 6501 hot wire anemometer product specification (KANOMAX 2019).

$$*\rho g_x - \frac{\partial P}{\partial x} + \mu \left(\frac{\partial^2 u}{\partial x^2} + \frac{\partial^2 u}{\partial y^2} + \frac{\partial^2 u}{\partial z^2} \right) = \rho \frac{\partial u}{\partial t}$$

$$*\rho g_y - \frac{\partial P}{\partial y} + \mu \left(\frac{\partial^2 v}{\partial x^2} + \frac{\partial^2 v}{\partial y^2} + \frac{\partial^2 v}{\partial z^2} \right) = \rho \frac{\partial v}{\partial t}$$

$$*\rho g_z - \frac{\partial P}{\partial z} + \mu \left(\frac{\partial^2 w}{\partial x^2} + \frac{\partial^2 w}{\partial y^2} + \frac{\partial^2 w}{\partial z^2} \right) = \rho \frac{\partial w}{\partial t}$$

$$\text{Cartesian: } \frac{\partial u}{\partial x} + \frac{\partial v}{\partial y} + \frac{\partial w}{\partial z} = 0$$

$$\text{Cylindrical: } \frac{1}{r} \frac{\partial}{\partial r} (r v_r) + \frac{1}{r} \frac{\partial}{\partial \theta} (v_\theta) + \frac{\partial}{\partial z} (v_z) = 0$$

* These are incompressible flow Navier Stokes equations. P , u , v , and w are unknowns which are combined with the incompressible flow continuity equation to form four equations with four unknowns (White 2011).

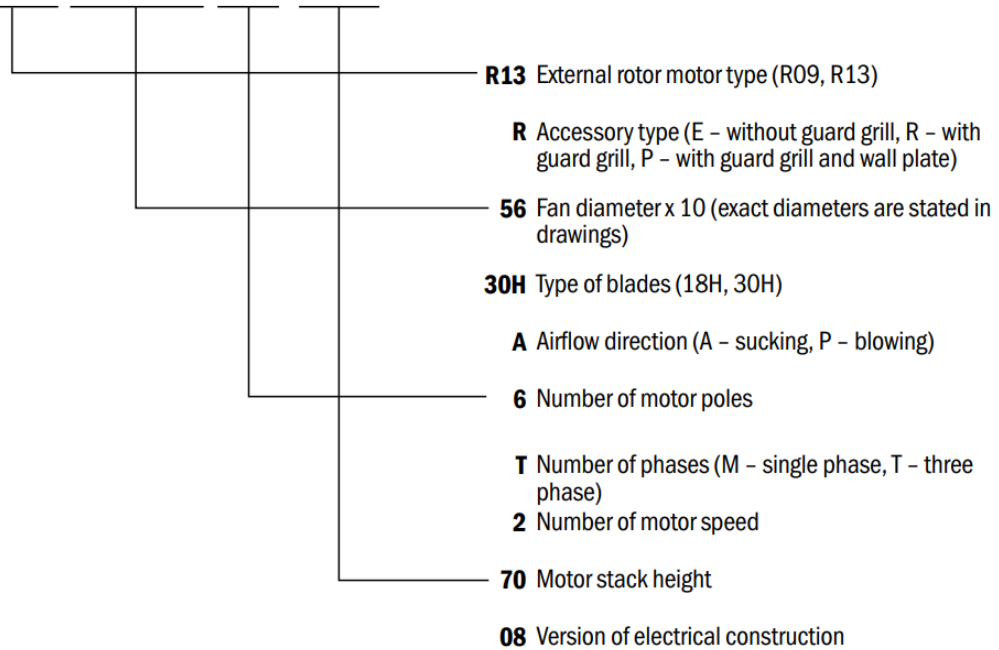
Example of type key:**R13R-5630HA-6T2-7008**

Figure B.4: Hidria axial fan ordering code (Hidria 2020).

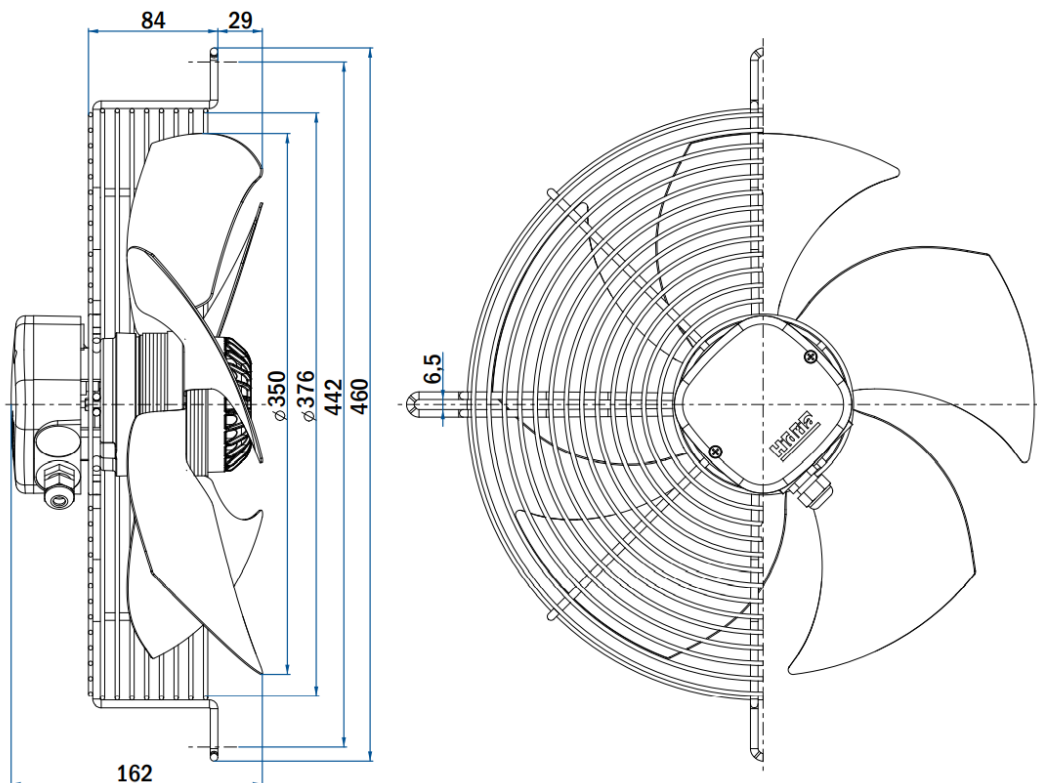


Figure B.5: Dimensions for Hidria axial fan 350 (mm) (Hidria 2020).

Nominal data according to standard EN 60335:	
Phase	1~
Nominal voltage	230 V
Frequency	50/60 Hz
Rated power input	130/165 W
Rated current	0.60/0.72 A
Rated speed	1290/1380 RPM
Min. ambient temperature	-30 °C
Max. ambient temperature	60 °C
Sound power level A weighted	72/75 dB (A)
Condensator	4 μ F/450 V
Connection	terminal box
Insulation class	155
Protection class	IP54

ErP data according to EU regulation 327/2011:	
Overall efficiency	29.0 %
Measurement category	A
Efficiency category	static
Efficiency grade N	40.7
Variable speed drive	NO
Power input	140 W
Air flow	1975 m ³ /h
Pressure drop	79 Pa
Speed	1333 RPM
Specific ratio	1.00

Figure B.6: Hidria axial fan 350 (mm) product specification (Hidria 2020).

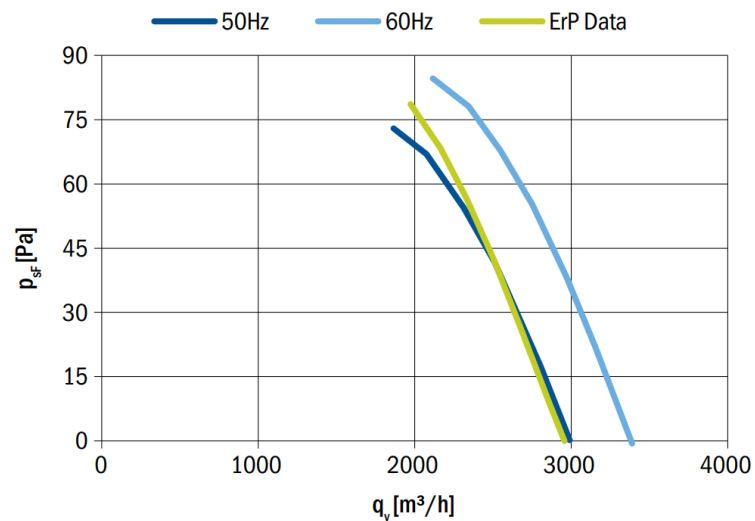


Figure B.7: Hidria axial fan 350 (mm) characteristic curve (Hidria 2020).

References

- Abu-Khadra, M. & Abofarha, F. (2019), Preliminary design of low speed wind tunnel, Technical report, FACULTY OF ENGINEERING AND INFORMATION TECHNOLOGY, AN-NAJAH NATIONAL UNIVERSITY (PALESTINE).
- Albertani, R., Stanford, B., Hubner, J. & Ifju, P. (2007), 'Aerodynamic coefficients and deformation measurements on flexible micro air vehicle wings', *Experimental Mechanics* **47**(5), 625–635.
- Baals, D. D. (1981), *Wind tunnels of NASA*, Vol. 440, Scientific and Technical Information Branch, National Aeronautics and Space
- Barlow, J. B., Rae, W. H. & Pope, A. (1999), *Low-speed wind tunnel testing*, John Wiley & sons.
- Batill, S. M. & Mueller, T. J. (1981), 'Visualization of transition in the flow over an airfoil using the smoke-wire technique', *AIAA journal* **19**(3), 340–345.
- Belaidouni, H., Samardžić, M. Đ., Jerković, D. D., Živković, S., Rajić, Z., Čurčić, D. & Kari, A. (2018), 'Comparison of static aerodynamic data obtained in dynamic wind tunnel tests and numerical simulation research', *Tehnički vjesnik* **25**(2), 445–452.
- Boutemedjet, A., Samardžić, M., Čurčić, D., Rajić, Z. & Ocokoljić, G. (2018), 'Wind tunnel measurement of small values of rolling moment using six-component strain gauge balance', *Measurement* **116**, 438–450.
- Calautit, J. K., Chaudhry, H. N., Hughes, B. R. & Sim, L. F. (2014), 'A validated design methodology for a closed-loop subsonic wind tunnel', *Journal of Wind Engineering and Industrial Aerodynamics* **125**, 180–194.
- Calautit, J. K. & Hughes, B. R. (2016), 'Cfd and experimental data of closed-loop wind tunnel flow', *Data in brief* **7**, 216–220.

- Dileep, G. S. & Raghavendra, N. V. (2018), *AERODYNAMICS LAB MANUAL*, INSTITUTE OF AERONAUTICAL ENGINEERING, INDIA.
- Fan, Z. (2010), 'Measurement of aerodynamic forces and moments in wind tunnels', *Encyclopedia of Aerospace Engineering*.
- Fluent (2017), 'Fluent tutorial guide [online]', Available at: <https://www.ansys.com/>. Retrieve on 7 March 2020.
- Gao, N. & Liu, X. (2018), 'An improved smoke-wire flow visualization technique using capacitor as power source', *Theoretical and Applied Mechanics Letters* **8**(6), 378–383.
- Garbeff, T. & Bell, J. (2019), 'Nasa ames unitary plan wind tunnel: Infrared flow visualization'.
- Gerhart, P. M., Gerhart, A. L. & Hochstein, J. I. (2016), *Munson, Young and Okiishi's Fundamentals of Fluid Mechanics*, John Wiley & Sons.
- Hanapur, I. & Gopalakrishna, S. (2016), 'Design optimization of 25mm diameter strain gauge balance for wind tunnel application', *International Journal for Innovative Research in Science and Technology* **3**(2), 464–469.
- Hidria (2020), 'Ac axial fans technical catalogue [online]', Available at: <https://www.hidria.com/>. Retrieve on 23 Oct 2020.
- Hufnagel, K. & Schewe, G. (2007), 'Force and moment measurement', *C. Tropea, A. L. Yarin, JF Foss, Springer Handbook of Experimental Fluid Mechanics* pp. 566–596.
- Jiang, F., Tai, Y.-C., Ho, C.-M., Karan, R. & Garstenauer, M. (1994), Theoretical and experimental studies of micromachined hot-wire anemometers, in 'Proceedings of 1994 IEEE International Electron Devices Meeting', IEEE, pp. 139–142.
- KANOMAX (2019), 'Climomaster model 6501 catalogue [online]', Available at: <https://www.kanomax-usa.com/>. Retrieve on 17 May 2020.
- Lerner, J. C. & Boldes, U. (2011), *Wind tunnels and experimental fluid dynamics research*, BoD–Books on Demand.
- Maeda, T., Kamada, Y., Murata, J., Yonekura, S., Ito, T., Okawa, A. & Kogaki, T. (2011), 'Wind tunnel study on wind and turbulence intensity profiles in wind turbine wake', *Journal of Thermal Science* **20**(2), 127–132.
- Merzkirch, W. (1987), Techniques of flow visualization, Technical report, ADVISORY GROUP FOR AEROSPACE RESEARCH AND DEVELOPMENT NEUILLY-SUR-SEINE (FRANCE).

- Moonen, P., Blocken, B., Roels, S. & Carmeliet, J. (2006), 'Numerical modeling of the flow conditions in a closed-circuit low-speed wind tunnel', *Journal of Wind Engineering and Industrial Aerodynamics* **94**(10), 699–723.
- NASA (2015), 'Open and closed return wind tunnel', Available at: <https://www.nasa.gov/>. Retrieve on 4 April 2020.
- Orellano, A. & Schober, M. (2006), Aerodynamic performance of a typical high-speed train, in 'Proceedings of the 4th WSEAS International Conference on Fluid Mechanics and Aerodynamics, Elounda, Greece', Citeseer, pp. 18–25.
- Post, F. H. & van Walsum, T. (1993), 'Fluid flow visualization, in focus on scientific visualization', *Springer Verlag, Berlin* pp. 1–40.
- Ristić, S. (2007), 'Flow visualisation techniques in wind tunnels part i–non optical methods', *Scientific Technical Review* **57**(1), 39–50.
- Ristić, S., Isaković, J., Ilić, B. & Ocokoljić, G. (2004), 'Review of methods for flow velocity measurement in wind tunnels', *Sci. Rev.* **54**(3).
- Samardžić, M., Anastasijević, Z., Marinkovski, D., Ćurčić, D. & Isaković, J. (2014), 'External six-component strain gauge balance for low speed wind tunnels', *Scientific Technical Review* **64**(3), 40–46.
- Sohankar, A., Mohagheghian, S., Dehghan, A. A. & Manshadi, M. D. (2015), 'A smoke visualization study of the flow over a square cylinder at incidence and tandem square cylinders', *Journal of Visualization* **18**(4), 687–703.
- Ștefănescu, D. M. (2020), *Handbook of Force Transducers: Characteristics and Applications*, Springer Nature.
- Systemair (2013), 'Axial fans catalogue [online]', Available at: <https://www.systemair.com/>. Retrieve on 21 April 2020.
- TecQuipment (2018), 'Three-component balance datasheet [online]', Available at: <https://www.tecquipment.com/>. Retrieve on 27 April 2020.
- White, F. M. (2011), *Fluid mechanics*, McGraw-hill.
- Yarusevych, S., Sullivan, P. E. & Kawall, J. G. (2009), 'Smoke-wire flow visualization in separated flows at relatively high velocities', *AIAA journal* **47**(6), 1592–1595.